

A stabilized cut discontinuous Galerkin framework: II. Hyperbolic problems

Ceren Gürkan^a, André Massing^{a,*}

^a*Department of Mathematics and Mathematical Statistics, Umeå University, SE-90187 Umeå, Sweden*

Abstract

We present the second part of a stabilized cut discontinuous Galerkin (cutDG) framework initiated in [1] and develop a novel cutDG method for scalar hyperbolic problems. The domain of interest is embedded into a structured, unfitted background mesh in \mathbb{R}^d where the domain boundary can cut through the mesh in an arbitrary fashion. To cope with robustness problems caused by small cut elements, we employ and extend ghost penalty techniques from recently developed, continuous cut finite element methods instead of the cell merging technique commonly used in unfitted discontinuous Galerkin methods, thus allowing for a minimal extension of existing fitted discontinuous Galerkin software to handle unfitted geometries. Identifying a few abstract assumptions on the ghost penalty, we derive geometrically robust a priori error and condition number estimates for the scalar hyperbolic problem which hold irrespective of the particular cut configuration. Possible realizations of suitable ghost penalties are discussed. The theoretical results are corroborated by a number of computational studies for various approximation orders and for two and three-dimensional test problems.

Keywords: hyperbolic problems, advection-dominated problems, discontinuous Galerkin, cut finite element method, stabilization, a priori error estimates, condition number

1. Introduction

1.1. Background and earlier work

The numerical solution of partial differential equations (PDEs) based on the finite element method requires the generation of high quality meshes to ensure both a proper geometric resolution of the domain features and good approximation properties of the numerical scheme. But even with today's advanced meshing techniques and continuously growing computer power, the generation of high quality meshes in realistic application problems can be a major bottleneck in the overall simulation pipeline. For instance, most traditional mesh-based numerical solution methods for geological flow and transport models require a series of highly complex preprocessing steps to translate geological image data into conforming domain discretizations which respect intricate geometric structures such as faults and large-scale networks of fractures [2]. Similar non-trivial preprocessing steps are necessary when mesh-based domain descriptions are extracted from biomedical image data [3, 4]. The problem of efficient and fast mesh generation becomes even more pronounced when the geometry of the model domain changes drastically in the course of the simulation. For instance, in fluid structure interaction problems [5–7], multiphase flows [8–11] or shape optimization problems [12–14], large or even topological changes in the model geometry may cause even state of the art mesh moving technologies to fail, leaving a costly remeshing as the only resort.

To ease the burden of mesh generation, novel so-called *unfitted* finite element methods have gained much attention in recent years, see [15] for a recent overview. In unfitted finite element

*Corresponding author

Email addresses: `ceren.gurkan@umu.se` (Ceren Gürkan), `andre.massing@umu.se` (André Massing)

methods, the mesh is exonerated from the task to represent the domain geometry accurately and only used to define proper approximation spaces. The geometry of the model domain is described independently by the means of a separate geometry model, e.g., a CAD or level-set based description, or even another, independently generated tessellation of the geometry boundary. Combined with suitable techniques to properly impose boundary or interface conditions, for instance by means of Lagrange multipliers or Nitsche-type methods [16–19], complex geometries can be simply embedded into an easy-to-generate background. As the embedded geometry can cut arbitrarily through the background mesh, a main challenge is to devise unfitted finite element methods that are geometrical robustness in the sense that standard a priori error and conditioning number estimates also hold in the unfitted case with constants independent of the particular cut configuration.

One possible solution to achieve geometrical robustness is provided by the approach taken in recent development of the *cut finite element method* (CutFEM). A distinctive feature of the cut finite element method is that it provides a general, theoretically founded stabilization framework which, roughly speaking, transfers stability and approximation properties from a finite element scheme posed on a standard mesh to its cut finite element counterpart. As a result, a wide range of problem classes has been treated including, e.g., elliptic interface problems [20–22], Stokes and Navier-Stokes type problems [23–31], two-phase and fluid-structure interaction problems [9, 32–34]. As a natural application area, unfitted finite element methods have also been proposed for problems in fractured porous media [35–38]. Finally, we also mention the finite cell method as another important instance of an unfitted finite element framework with applications to flow and mechanics problems [39–41], see [42] for a review and references therein.

In addition to the aforementioned unfitted *continuous* finite element methods, unfitted *discontinuous Galerkin* (DG) methods have successfully been devised to treat boundary and interface problems on complex and evolving domains [43–45], including flow problems with moving boundaries and interfaces [46–51]. In contrast to stabilized continuous cut finite element methods, in unfitted discontinuous Galerkin methods, troublesome small cut elements can be merged with neighbor elements with a large intersection support by simply extending the local shape functions from the large element to the small cut element. As inter-element continuity is enforced only weakly, no additional measures need to be taken to force the modified basis functions to be globally continuous. Consequently, cell merging in unfitted discontinuous Galerkin methods provides an alternative stabilization mechanism to ensure that the discrete systems are well-posed and well-conditioned. For a very recent extension of the cell merging approach to continuous finite elements, we refer to [52, 53]. Thanks to their favorable conservation and stability properties, unfitted discontinuous Galerkin methods remain an attractive alternative to continuous CutFEMs, but some drawbacks are the almost complete absence of numerical analysis except for [54, 55], the implementational labor to track changing matrix sparsity patterns when merging cut elements, and the lack of natural discretization approaches for PDEs defined on surfaces.

So far, most of the theoretically analyzed unfitted finite element schemes have been proposed for elliptic type of problems. Much less attention has been paid to the theoretical development of unfitted finite element methods for advection-dominant or hyperbolic problems, except for [27, 28] considering a continuous interior penalty (CIP) based CutFEM for the Oseen problem, and [56–58] developing continuous unfitted finite element methods for advection–diffusion equations on surfaces based on the CIP and streamline upwind Petrov Galerkin (SUPG) approach. On the other hand, for the DG community, hyperbolic problems have been of interest from the very beginning, as the first DG method was developed by Reed and Hill [59] to model neutron transport problem. The very first analysis of these methods was presented in [60] and then improved in [61], while Brezzi et al. [62] reformulated and generalized the upwind flux strategy in DG methods for hyperbolic problems by introducing a tunable penalty parameter. The tempting conservation and stability properties, the high locality and particularly the naturally inherited upwind flux term in the bilinear form makes DG methods popular to handle specifically advection dominated problems [63–65] as well as elliptic ones [66, 67]. As the literature on DG methods for both elliptic and hyperbolic problems is vast, we do not attempt to give a detailed overview but rather refer to the excellent monographs [68, 69], which also includes comprehensive bibliographies.

1.2. Novel contributions and outline of this paper

In this work we continue the development of a novel *stabilized* cut discontinuous Galerkin (cutDG) framework initiated in [1]. Departing from the elliptic boundary and interface problems considered in [1], we here propose and analyze a cutDG method for scalar hyperbolic equations. In the upcoming work [70], we will combine the presented framework with extension of [71, 72] to introduce cutDGM for mixed-dimensional, coupled problems. The idea of extending stabilization techniques from the continuous CutFEM approach [73] to discontinuous Galerkin based discretizations allows for a minimally invasive extension of existing fitted discontinuous Galerkin software to handle unfitted geometries. Only additional quadrature routines need to be added to handle the numerical integration on cut geometries, and while not being a completely trivial implementation task, we refer to the numerous quadrature algorithms capable of higher order geometry approximation [45, 74–77] which have been proposed in recent years. With a suitable choice of the ghost penalty, the sparsity pattern associated with the final system matrix does not require any manipulation and is identical to its fitted DG counterpart.

We start by briefly recalling the advection-reaction model problem and its corresponding weak formulation in Section 2, followed by the presentation of the stabilized cut discontinuous Galerkin method in Section 3 which includes an additional abstract ghost penalty. A main feature of the presented numerical analysis is that we identify a number of abstract assumptions on the ghost penalty to prove geometrically robust optimal a priori error and condition number estimates which hold independent of the particular cut configuration. To prepare the a priori error analysis, Section 4 collects a number of useful inequalities and explains the construction of an unfitted but stable L^2 projection operator. In Section 5, we derive an inf-sup condition in a ghost penalty enhanced streamline-diffusion type norm. A key observation is that the classical argument in [62] based on boundedness on orthogonal subscales does not work as the local orthogonality properties of the unfitted L^2 projection is perturbed due to the mismatch of the physical domain and the active mesh where the discontinuous ansatz functions are defined. In Section 6, the results from the previous sections are combined to establish an optimal a priori error estimate for the proposed stabilized cutDG method with constants independent of the particular cut configuration. We continue our abstract analysis in Section 7 and prove that condition number scales like $\mathcal{O}(h^{-1})$, again with geometrically robust constants. Our theoretical investigation concludes with discussing a number of ghost penalty realizations in Section 8. Finally, we corroborate our theoretical analysis with numerical examples in Section 9 where we study both the convergence properties and geometrical robustness of the proposed cutDG method.

1.3. Basic notation

Throughout this work, $\Omega \subset \mathbb{R}^d$, $d = 2, 3$ denotes an open and bounded domain with piecewise smooth boundary $\partial\Omega$, while $\Gamma = \partial\Omega$ denotes its topological boundary. For $U \in \{\Omega, \Gamma\}$ and $0 \leq m < \infty$, $1 \leq q \leq \infty$, let $W^{m,q}(U)$ be the standard Sobolev spaces consisting of those \mathbb{R} -valued functions defined on U which possess L^q -integrable weak derivatives up to order m . Their associated norms are denoted by $\|\cdot\|_{m,q,U}$. As usual, we write $H^m(U) = W^{m,2}(U)$ and $(\cdot, \cdot)_{m,U}$ and $\|\cdot\|_{m,U}$ for the associated inner product and norm. If unmistakable, we occasionally write $(\cdot, \cdot)_U$ and $\|\cdot\|_U$ for the inner products and norms associated with $L^2(U)$, with U being a measurable subset of \mathbb{R}^d . Any norm $\|\cdot\|_{\mathcal{P}_h}$ used in this work which involves a collection of geometric entities \mathcal{P}_h should be understood as broken norm defined by $\|\cdot\|_{\mathcal{P}_h}^2 = \sum_{P \in \mathcal{P}_h} \|\cdot\|_P^2$ whenever $\|\cdot\|_P$ is well-defined, with a similar convention for scalar products $(\cdot, \cdot)_{\mathcal{P}_h}$. Any set operations involving \mathcal{P}_h are also understood as element-wise operations, e.g., $\mathcal{P}_h \cap U = \{P \cap U \mid P \in \mathcal{P}_h\}$ and $\partial\mathcal{P}_h = \{\partial P \mid P \in \mathcal{P}_h\}$ allowing for compact short-hand notation such as $(v, w)_{\mathcal{P}_h \cap U} = \sum_{P \in \mathcal{P}_h} (v, w)_{P \cap U}$ and $\|\cdot\|_{\partial\mathcal{P}_h \cap U} = \sqrt{\sum_{P \in \mathcal{P}_h} \|\cdot\|_{\partial P \cap U}^2}$. Finally, throughout this work, we use the notation $a \lesssim b$ for $a \leq Cb$ for some generic constant C (even for $C = 1$) which varies with the context but is always independent of the mesh size h and the position of Γ relative to the background \mathcal{T}_h , but may be dependent on the dimensions d , the polynomial degree of the finite element functions, the shape regularity of the mesh and the curvature of Γ .

2. Model problem

For a given vector field $b \in [W^{1,\infty}(\Omega)]^d$ and a scalar function $c \in L^\infty(\Omega)$ we consider the advection-reaction problem of the form

$$b \cdot \nabla u + cu = f \quad \text{in } \Omega, \quad (2.1a)$$

$$u = g \quad \text{on } \Gamma^-, \quad (2.1b)$$

where $g \in L^2(\Gamma^-)$ describes the boundary value on the inflow boundary of Ω defined by

$$\Gamma^- = \{x \in \partial\Omega \mid b(x) \cdot n_\Gamma(x) < 0\}. \quad (2.2)$$

Here, n_Γ denotes the outer normal associated with Γ . Correspondingly, the outflow and characteristic boundary are defined by, respectively,

$$\Gamma^+ = \{x \in \partial\Omega \mid b(x) \cdot n_\Gamma(x) > 0\}, \quad (2.3)$$

$$\Gamma^0 = \{x \in \partial\Omega \mid b(x) \cdot n_\Gamma(x) = 0\}. \quad (2.4)$$

As usual in this setting, we assume that

$$c_0 := \operatorname{ess\,inf}_{x \in \Omega} \left(c(x) - \frac{1}{2} \nabla \cdot b(x) \right) > 0. \quad (2.5)$$

The corresponding weak formulation of scalar hyperbolic problem (2.1) is to seek $u \in V := \{v \in L^2(\Omega) \mid b \cdot \nabla v \in L^2(\Omega)\}$ such that $\forall v \in V$

$$a(u, v) = l(v), \quad (2.6)$$

with the bilinear form $a(\cdot, \cdot)$ and linear form $l(\cdot)$ given by

$$a(u, v) = (b \cdot \nabla u + cu, v)_\Omega - (b \cdot n_\Gamma u, v)_{\Gamma^-}, \quad l(v) = (f, v)_\Omega - (b \cdot n_\Gamma g, v)_{\Gamma^-}. \quad (2.7)$$

3. A cut discontinuous Galerkin method for the advection-reaction problem

Let $\tilde{\mathcal{T}}_h$ be a background mesh consisting of d -dimensional, shape-regular (closed) simplices $\{T\}$ covering $\bar{\Omega}$. As usual, we introduce the local mesh size $h_T = \operatorname{diam}(T)$ and the global mesh size $h = \max_{T \in \tilde{\mathcal{T}}_h} \{h_T\}$. For $\tilde{\mathcal{T}}_h$ we define the so-called *active mesh*

$$\mathcal{T}_h = \{T \in \tilde{\mathcal{T}}_h \mid T \cap \Omega^\circ \neq \emptyset\}, \quad (3.1)$$

and its submesh \mathcal{T}_Γ consisting of all elements cut by the boundary,

$$\mathcal{T}_\Gamma = \{T \in \mathcal{T}_h \mid T \cap \Gamma \neq \emptyset\}. \quad (3.2)$$

Note that since the elements $\{T\}$ are closed by definition, the active mesh \mathcal{T}_h still covers Ω . The set of interior faces in the active background mesh is given by

$$\mathcal{F}_h = \{F = T^+ \cap T^- \mid T^+, T^- \in \mathcal{T}_h\}. \quad (3.3)$$

To keep the technical details the forthcoming numerical analysis at a moderate level, we make two reasonable geometric assumptions on \mathcal{T}_h and Γ .

Assumption G1. *The mesh \mathcal{T}_h is quasi-uniform.*

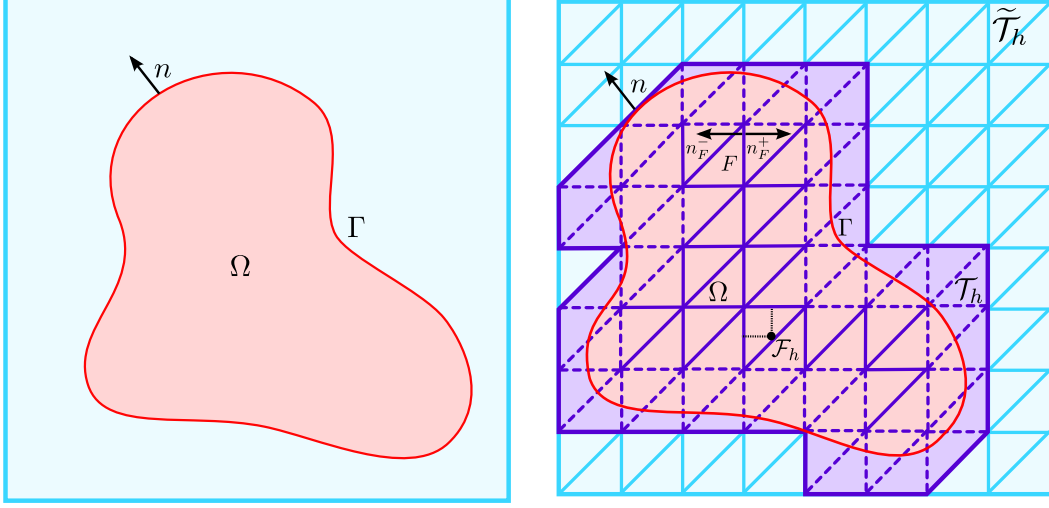


Figure 3.1: Computational domains for the boundary value problem (2.1). (Left) Physical domain Ω with boundary Γ and outer normal n . (Right) Background mesh and active mesh used to define the approximation space. Dashed faces are used to define face based ghost penalties discussed in Section 8.

Assumption G2. For $T \in \mathcal{T}_\Gamma$ there is an element T' in $\omega(T)$ with a “fat” intersection¹ such that

$$|T' \cap \Omega|_d \geq c_s |T'|_d \quad (3.4)$$

for some mesh independent $c_s > 0$. Here, $\omega(T)$ denotes the set of elements sharing at least one node with T .

Remark 3.1. Quasi-uniformity of \mathcal{T}_h is assumed mostly for notational convenience. Except for the condition number estimates, all derived estimates can be easily localized to element or patch-wise estimates.

Remark 3.2. The “fat” intersection property guarantees that Γ is reasonably resolved by the active mesh \mathcal{T}_h . It is automatically satisfied if, e.g., $\Gamma \in C^2$ and h is small enough, that is; if $h \lesssim \min_{\{1, \dots, d-1\}} \|\frac{1}{\kappa_i}\|_{L^\infty(\Gamma)}$ where $\{\kappa_1, \dots, \kappa_{d-1}\}$ are the principal curvatures of Γ , see [22].

On the active mesh \mathcal{T}_h , we define the discrete function space V_h as the broken polynomial space of order p ,

$$V_h := \mathbb{P}_p(\mathcal{T}_h) := \bigoplus_{T \in \mathcal{T}_h} \mathbb{P}_p(T). \quad (3.5)$$

To formulate our cut discontinuous Galerkin discretization of the weak problem (2.6), we recall the usual definitions of the averages

$$\{\sigma\}_F = \frac{1}{2}(\sigma_F^+ + \sigma_F^-), \quad (3.6)$$

$$\{n_F \cdot \sigma\}_F = \frac{1}{2}n_F \cdot (\sigma_F^+ + \sigma_F^-), \quad (3.7)$$

and the jump across an interior facet $F \in \mathcal{F}_h$,

$$[w]_F = w_F^+ - w_F^-. \quad (3.8)$$

Here, $w_F^\pm(x) = \lim_{t \rightarrow 0^+} w(x \pm tn_F)$ for some chosen unit facet normal n_F on F .

¹The constant c_s is typically user-defined.

Remark 3.3. To keep the notation at a moderate level, we will from hereon drop any subscripts indicating whether a normal belongs to a face F or to the boundary Γ as it will be clear from context.

With these definitions in place, our cut discontinuous Galerkin method for advection-reaction problem (2.1) can be formulated as follows: find $u_h \in V_h$ such that $\forall v \in V_h$

$$A_h(u_h, v) := a_h(u_h, v) + g_h(u_h, v) = l_h(v). \quad (3.9)$$

The discrete bilinear forms $a_h(\cdot, \cdot)$ and $l_h(\cdot)$ represent the classical discrete, discontinuous Galerkin counterparts of (2.6) defined on mesh elements and faces restricted to the physical domain Ω . More precisely, for $v, w \in V_h$, we let

$$\begin{aligned} a_h(v, w) &= (b \cdot \nabla v + cv, w)_{\mathcal{T}_h \cap \Omega} - (b \cdot nv, w)_{\Gamma^-} \\ &\quad - (b \cdot n[v], \{w\})_{\mathcal{F}_h \cap \Omega} + \frac{1}{2}(|b \cdot n|[v], [w])_{\mathcal{F}_h \cap \Omega}, \end{aligned} \quad (3.10)$$

$$l_h(w) = (f, w)_{\Omega} - (b \cdot ng, w)_{\Gamma^-}. \quad (3.11)$$

The main difference to the classical discontinuous Galerkin method for Problem (2.1), cf. [62, 68], is the appearance of an additional stabilization form g_h , also known as *ghost penalty*. The role of the ghost penalty is to ensure that the favorable stability and approximation properties of the classical upwind stabilized discontinuous Galerkin method carry over to the unfitted mesh scenario. The precise requirements on g_h will be formulated as a result of the theoretical analysis performed in the remaining sections, but we already point out that since Problem (2.1) involves an advection and a reaction term, it will be natural to assume that g_h can be decomposed in a reaction related ghost penalty g_c and an advection related ghost penalty g_b , both of which we assume to be symmetric,

$$g_h(v, w) = g_c(v, w) + g_b(v, w) \quad \forall v, w \in V_h. \quad (3.12)$$

4. Norms, useful inequalities and approximation properties

Following the presentation in [68], we introduce a reference velocity b_c and a reference time τ_c ,

$$b_c = \|b\|_{0,\infty,\Omega}, \quad \tau_c^{-1} = \|c\|_{0,\infty,\Omega} + |b|_{1,\infty,\Omega}, \quad (4.1)$$

and define the central flux, upwind and the scaled streamline diffusion norm by setting

$$|||v|||_{\text{cf}}^2 = \tau_c^{-1} \|v\|_{\Omega}^2 + \frac{1}{2} \| |b \cdot n|^{1/2} v \|_{\Gamma}^2, \quad (4.2)$$

$$|||v|||_{\text{up}}^2 = |||v|||_{\text{cf}}^2 + \frac{1}{2} \| |b \cdot n|^{1/2} [v] \|_{\mathcal{F}_h \cap \Omega}^2, \quad (4.3)$$

$$|||v|||_{\text{sd}}^2 = |||v|||_{\text{up}}^2 + \|\phi_b^{1/2} b \cdot \nabla v\|_{\mathcal{T}_h \cap \Omega}^2, \quad (4.4)$$

respectively. Thanks to the assumed quasi-uniformity, the global scaling factor ϕ_b is given by

$$\phi_b = h/b_c. \quad (4.5)$$

For each norm $||| \cdot |||_t$ with $t \in \{\text{cf}, \text{up}, \text{sd}\}$, its ghost penalty enhanced version is given by

$$|||v|||_{t,h} = |||v|||_t^2 + |v|_{g_h}^2. \quad (4.6)$$

To simplify a number of estimates, we will also use a slightly stronger norm than $||| \cdot |||_{\text{sd},h}$, namely

$$|||v|||_{\text{sd},h,*}^2 = |||v|||_{\text{cf}}^2 + \|\phi_b^{1/2} b \cdot \nabla v\|_{\mathcal{T}_h \cap \Omega}^2 + b_c \|v\|_{\partial \mathcal{T}_h \cap \Omega}^2 + |v|_{g_h}^2. \quad (4.7)$$

Finally, we assume as in [68] that the mesh \mathcal{T}_h is sufficiently resolved such that the inequality

$$h \leq b_c \tau_c \quad (4.8)$$

is satisfied, which means that Problem (2.1) can be considered as advection dominant and that the advective velocity field b is sufficiently resolved in the sense that the following estimates hold,

$$\|c\|_{0,\infty,\Omega} h \leq b_c, \quad |b|_{1,\infty,\Omega} \leq \frac{b_c}{h}. \quad (4.9)$$

Before we turn to the stability and a prior error analysis in Section 5, we briefly review some useful inequalities needed later and explain how a suitable approximation operator can be constructed on the active mesh \mathcal{T}_h . Recall that for $v \in H^1(\mathcal{T}_h)$, the local trace inequalities of the form

$$\|v\|_{\partial T} \lesssim h^{-1/2} \|v\|_T + h^{1/2} \|\nabla v\|_T \quad \forall T \in \mathcal{T}_h, \quad (4.10)$$

$$\|v\|_{\Gamma \cap T} \lesssim h^{-1/2} \|v\|_T + h^{1/2} \|\nabla v\|_T \quad \forall T \in \mathcal{T}_h, \quad (4.11)$$

hold, see [78] for a proof of the second one. For $v_h \in V_h$, let D^j be the j -th total derivative, then the following inverse inequalities hold,

$$\|D^j v_h\|_{T \cap \Omega} \lesssim h^{i-j} \|D^i v_h\|_T \quad \forall T \in \mathcal{T}_h, \quad 0 \leq i \leq j, \quad (4.12)$$

$$\|D^j v_h\|_{\partial T \cap \Omega} \lesssim h^{i-j-1/2} \|D^i v_h\|_T \quad \forall T \in \mathcal{T}_h, \quad 0 \leq i \leq j, \quad (4.13)$$

$$\|D^j v_h\|_{\Gamma \cap T} \lesssim h^{i-j-1/2} \|D^i v_h\|_T \quad \forall T \in \mathcal{T}_h, \quad 0 \leq i \leq j, \quad (4.14)$$

see [78] for a proof of the last one. Next, to define a suitable approximation operator, we depart from the L^2 -orthogonal projection $\pi_h : L^2(\mathcal{T}_h) \rightarrow V_h$ which for $T \in \mathcal{T}_h$ and $F \in \mathcal{F}_T$ satisfies the error estimates

$$|v - \pi_h v|_{T,r} \lesssim h_T^{s-r} |v|_{s,T}, \quad 0 \leq r \leq s, \quad (4.15)$$

$$|v - \pi_h v|_{F,r} \lesssim h_T^{s-r-1/2} |v|_{s,T}, \quad 0 \leq r \leq s - 1/2, \quad (4.16)$$

whenever $v \in H^s(T)$. Now to lift a function $v \in H^s(\Omega)$ to $H^s(\Omega_h^e)$, where we for the moment use the notation $\Omega_h^e = \bigcup_{T \in \mathcal{T}_h} T$, we recall that for Sobolev spaces $W^{m,q}(\Omega)$, $0 < m \leq \infty$, $1 \leq q \leq \infty$, there exists a bounded extension operator satisfying

$$(\cdot)^e : W^{m,q}(\Omega) \rightarrow W^{m,q}(\mathbb{R}^d), \quad \|v^e\|_{m,q,\mathbb{R}^d} \lesssim \|v\|_{m,q,\Omega} \quad (4.17)$$

for $u \in W^{m,q}(\Omega)$, see [79] for a proof. We can now define an unfitted L^2 projection variant $\pi_h^e : H^s(\Omega_h^e) \rightarrow V_h$ by setting

$$\pi_h^e v := \pi_h v^e. \quad (4.18)$$

Note that this L^2 -projection is slightly perturbed in the sense that it is not orthogonal on $L^2(\Omega)$ but rather on $L^2(\Omega_h^e)$. Combining the local approximation properties of π_h with the stability of the extension operator $(\cdot)^e$, we see immediately that π_h^e satisfies the global error estimates

$$\|v - \pi_h^e v\|_{\mathcal{T}_h,r} \lesssim h^{s-r} \|v\|_{s,\Omega}, \quad 0 \leq r \leq s, \quad (4.19)$$

$$\|v - \pi_h^e v\|_{\mathcal{F}_h,r} \lesssim h^{s-r-1/2} \|v\|_{s,\Omega}, \quad 0 \leq r \leq s - 1/2, \quad (4.20)$$

$$\|v - \pi_h^e v\|_{\Gamma,r} \lesssim h^{s-r-1/2} \|v\|_{s,\Omega}, \quad 0 \leq r \leq s - 1/2. \quad (4.21)$$

To assure that the consistency error caused by g_h does not affect the convergence order, we require that the ghost penalties g_b and g_c are weakly consistent in the following sense.

Assumption HP1 (Weak consistency estimate). For $u \in H^s(\Omega)$ and $r = \min\{s, p+1\}$, the semi-norms $|\cdot|_{g_b}$ and $|\cdot|_{g_c}$ satisfy the estimates

$$|\pi_h^e u|_{g_b} \lesssim b_c^{1/2} h^{r-1/2} \|u\|_{r,\Omega}, \quad (4.22)$$

$$|\pi_h^e u|_{g_c} \lesssim \tau_c^{-1/2} h^r \|u\|_{r,\Omega}. \quad (4.23)$$

With these assumptions, the approximation error of the unfitted L^2 projection can be quantified with respect to the $||| \cdot |||_{\text{sd},h,*}$ norm.

Proposition 4.1. Let $u \in H^s(\Omega)$ and assume that $V_h = \mathbb{P}_p(\mathcal{T}_h)$. Then for $r = \min\{s, p+1\}$, the approximation error of π_h^e satisfies

$$|||u - \pi_h^e u|||_{\text{sd},h,*} \lesssim (\tau_c^{-1/2} h^{1/2} + b_c^{1/2} h^{r-1/2}) \|u\|_{r,\Omega}. \quad (4.24)$$

PROOF. Set $e_\pi = u - \pi_h^e u$, then by definition

$$|||e_\pi|||_{\text{sd},h,*}^2 = \tau_c^{-1} \|e_\pi\|_\Omega^2 + \frac{1}{2} |||b \cdot n|^{1/2} e_\pi|||_\Gamma^2 + b_c \|e_\pi\|_{\partial\mathcal{T}_h \cap \Omega}^2 + \|\phi_b^{1/2} b \cdot \nabla e_\pi\|_\Omega^2 + |e_\pi|_{g_h}^2 \quad (4.25)$$

$$= I + II + III + IV + |e_\pi|_{g_h}^2. \quad (4.26)$$

Thanks to Assumption HP1, we only need to estimate I – IV . Using (4.19), I is bounded by

$$I \lesssim \tau_c^{-1} h^{2r} \|u\|_{r,\Omega}^2, \quad (4.27)$$

while the last three terms can be bounded by combining (4.19)–(4.21) leading to

$$II + III + IV \lesssim b_c \|h^{-1/2} e_\pi\|_{\mathcal{T}_h}^2 + b_c \|h^{1/2} \nabla e_\pi\|_{\mathcal{T}_h}^2 \lesssim b_c h^{2r-1} \|u\|_{r,\Omega}^2. \quad (4.28)$$

□

5. Stability analysis

The goal of this section is show that the stabilized cutDG method (3.9) satisfies a discrete inf-sup condition with respect to the $||| \cdot |||_{\text{sd},h}$ -norm, similar to the results presented in [68, 80] for the corresponding classical fitted discontinuous Galerkin method. In the unfitted case, one main challenge is that the proof of the inf-sup condition involves various inverse estimates which in turn forces us to gain control over the considered $||| \cdot |||_{\text{sd}}$ norm on the entire active mesh.

We start our theoretical analysis by recalling that a partial integration of the element contributions in bilinear form (3.10) leads to a mathematically equivalent expression for a_h , namely,

$$\begin{aligned} a_h(v, w) &= ((c - \nabla \cdot b)v, w)_{\mathcal{T}_h \cap \Omega} - (v, b \cdot \nabla w)_{\mathcal{T}_h \cap \Omega} + (b \cdot nv, w)_\Gamma + \\ &\quad + (b \cdot n\{v\}, [w])_{\mathcal{F}_h \cap \Omega} + \frac{1}{2} (|b \cdot n|[v], [w])_{\mathcal{F}_h \cap \Omega}. \end{aligned} \quad (5.1)$$

By taking the average of (3.10) and (5.1), we obtain the well-known decomposition of $a_h(\cdot, \cdot)$ into a symmetric and skew-symmetric part,

$$a_h(v, w) = a_h^{\text{sy}}(v, w) + a_h^{\text{sk}}(v, w), \quad (5.2)$$

where

$$a_h^{\text{sy}}(v, w) = (c - \frac{1}{2} \nabla \cdot b)v, w)_{\mathcal{T}_h \cap \Omega} + \frac{1}{2} (|b \cdot n|v, w)_\Gamma + \frac{1}{2} (|b \cdot n|[v], [w])_{\mathcal{F}_h \cap \Omega}, \quad (5.3)$$

$$a_h^{\text{sk}}(v, w) = \frac{1}{2} ((b \cdot \nabla v, w)_{\mathcal{T}_h \cap \Omega} - (v, b \cdot \nabla w)_{\mathcal{T}_h \cap \Omega} \quad (5.4)$$

$$- (b \cdot n[v], \{w\})_{\mathcal{F}_h \cap \Omega} + (b \cdot n\{v\}, [w])_{\mathcal{F}_h \cap \Omega}). \quad (5.5)$$

Consequently, the total bilinear form $A_h(\cdot, \cdot)$ is discretely coercive with respect to $||| \cdot |||_{\text{up},h}$:

Lemma 5.1. *For $v \in V_h$ it holds*

$$c_0 \tau_c \|v\|_{\text{up},h}^2 \lesssim A_h(v_h, v_h). \quad (5.6)$$

PROOF. As in the classical fitted mesh case, the proof follows simply from observing that

$$A_h(v, v) = a_h(v, v) + g_h(v, v) = a_h^{\text{sy}}(v, v) + g_h(v, v) \quad (5.7)$$

$$\geq c_0 \|v\|_{\mathcal{T}_h \cap \Omega}^2 + \frac{1}{2} \|b \cdot n|^{1/2} v\|_{\Gamma} + \frac{1}{2} \|b \cdot n|^{1/2} v\|_{\mathcal{F}_h \cap \Omega} + |v|_{g_h} \gtrsim c_0 \tau_c \|v\|_{\text{up},h}^2, \quad (5.8)$$

noting that $0 < c_0 \tau_c \lesssim 1$ thanks to assumption (2.5) and the definition of τ_c , cf. (4.1). \square

Remark 5.2. We point out that for the advection-reaction problem, the ghost penalty g_h is not needed to establish discrete coercivity in the $\|\cdot\|_{\text{up},h}$ norm, in contrast to the cutDGM for the Poisson problem presented in [1]. Nevertheless, we will see that g_h is required to prove an inf-sup condition for the discrete problem (3.9) using the stronger $\|\cdot\|_{\text{sd},h}$ norm.

Following the derivation of the inf-sup condition in the fitted mesh case, see for instance [81], a proper test function $v \in V_h$ needs to be constructed which establishes control over the streamline derivative. To construct such a suitable test function, we assume the existence of discrete vector field $b_h \in \mathbb{P}_0(\mathcal{T}_h)$ satisfying

$$\|b_h^0 - b\|_{0,\infty,T} \lesssim h_T |b|_{1,\infty,T}, \quad \|b_h^0\|_{0,\infty,T} \lesssim \|b^e\|_{0,\infty,T}. \quad (5.9)$$

Note that for $b \in [W^{1,\infty}(\Omega)]$ such a discrete vector field b_h^0 can always be constructed. To establish the inf-sup result, the ghost penalties g_b and g_c for the discretized advection-reaction problem are supposed to satisfy the following assumptions.

Assumption HP2. *The ghost penalty g_c extends the L^2 norm from the physical domain Ω to the active mesh in the sense that for $v_h \in V_h$, it holds that*

$$\tau_c^{-1} \|v\|_{\mathcal{T}_h}^2 \lesssim \tau_c^{-1} \|v\|_{\Omega}^2 + |v|_{g_c}^2 \lesssim \tau_c^{-1} \|v\|_{\mathcal{T}_h}^2. \quad (5.10)$$

Assumption HP3. *The ghost penalty g_b extends the streamline diffusion semi-norm from the physical domain Ω to the active mesh in the sense that for $v_h \in V_h$, it holds that*

$$\|\phi_b^{1/2} b \cdot \nabla v\|_{\mathcal{T}_h}^2 \lesssim \|\phi_b^{1/2} b \cdot \nabla v\|_{\Omega}^2 + |v|_{g_b}^2 + \tau_c^{-1} \|v\|_{\Omega}^2 + |v|_{g_c}^2 \lesssim \|\phi_b^{1/2} b \cdot \nabla v\|_{\mathcal{T}_h}^2 + \tau_c^{-1} \|v\|_{\mathcal{T}_h}^2. \quad (5.11)$$

Remark 5.3. At first it might be more natural to assume that

$$\|\phi_b^{1/2} b \cdot \nabla v\|_{\mathcal{T}_h}^2 \sim \|\phi_b^{1/2} b \cdot \nabla v\|_{\Omega}^2 + |v|_{g_b}^2 \quad (5.12)$$

is valid for $v \in V_h$ instead of the more convoluted estimate (5.11), but the forthcoming numerical analysis as well as the actual design of g_b will require to frequently pass between certain locally constructed discrete vector fields b_h and the original vector field b . This is also the content of the next lemma.

Lemma 5.4. *Let $v \in V_h$ and let $P \subset \mathcal{T}_h$ be an element patch with $\text{diam}(P) \sim h$. Let b_h^P be a patch-wide defined velocity field satisfying*

$$\|b_h^P - b\|_{0,\infty,P} \lesssim h |b^e|_{1,\infty,P}, \quad \|b_h^P\|_{0,\infty,P} \lesssim \|b^e\|_{0,\infty,P}. \quad (5.13)$$

Then

$$\phi_b \|b_h^P - b\|_P^2 \|\nabla v\|_P^2 \lesssim \tau_c^{-1} \|v\|_P^2. \quad (5.14)$$

Before we turn to proof we note an immediate corollary of Lemma 5.4 and Assumption HP3.

Corollary 5.5. *Let \mathcal{P}_h be a collection of patches and assume that the number of patch overlaps is uniformly bounded. Let b_h^P and $P \in \mathcal{P}_h$ satisfy the assumptions in Lemma 5.4. Then*

$$\|\phi_b^{1/2} b_h^P \cdot \nabla v\|_{\mathcal{P}_h}^2 \lesssim \|v\|_{\text{up},h}^2. \quad (5.15)$$

PROOF (LEMMA 5.4). Thanks to the assumptions (5.13) and the fact that $\phi_b \|b\|_{0,\infty,P} \lesssim h$, we have the following chain of estimates,

$$\phi_b \|b_h - b\|_{0,\infty,P}^2 \lesssim \phi_b \|b\|_{0,\infty,P} h \|b\|_{1,\infty,P} \lesssim h^2 \|b\|_{1,\infty,P}. \quad (5.16)$$

Thus an application of the Cauchy-Schwarz inequality and the inequality (4.12) to $\|\nabla v\|_P$ yields

$$\|\phi_b^{1/2} (b_h^P - b) \cdot \nabla v\|_P^2 \lesssim \phi_b \|b_h^P - b\|_{0,\infty,P}^2 \|\nabla v\|_P^2 \lesssim \|b\|_{1,\infty,\Omega} h^2 \|\nabla v\|_P^2 \lesssim \tau_c^{-1} \|v\|_P^2. \quad (5.17)$$

□

Remark 5.6. Note that thanks to assumption $b \in W^{1,\infty}(\Omega)$ and the existence of an extension operator $(\cdot)^e : W^{1,\infty}(\Omega) \rightarrow W^{1,\infty}(\mathbb{R}^d)$, cf. Section 4, a patch-wise defined velocity field b_h^P satisfying Lemma 5.4, Eq. (5.13) can be always constructed, e.g., by simply taking the value of b at some point in the patch.

Next, we state and prove the main result of this section, showing that the cut discontinuous Galerkin method (3.9) for the advection-reaction problem (2.1) is inf-sup stable with respect to the $\|\cdot\|_{\text{sd},h}$ norm. The main challenge here is to show that this result holds with a stability constant which is independent of the particular cut configuration.

Theorem 5.7. *Let A_h be the bilinear form defined by (3.9). Then for $v \in V_h$ it holds that*

$$c_0 \tau_c \|v\|_{\text{sd},h} \lesssim \sup_{w \in V_h \setminus \{0\}} \frac{A_h(v, w)}{\|w\|_{\text{sd},h}}. \quad (5.18)$$

with the hidden constant independent of the particular cut configuration.

PROOF. We follow the proof for the fitted DG method, see for instance [68], to construct a suitable test function $w \in V_h$ for given $v \in V_h$ such that (5.18) holds.

Step 1. Setting $w_1 = v$, we gain control over the $\|w\|_{\text{up},h}^2$, thanks to the coercivity result (5.6),

$$A_h(v, w_1) \geq c_0 \tau_c \|v\|_{\text{up},h}^2. \quad (5.19)$$

Step 2. Next, set $w_2 = \phi_b b_h^0 \nabla v$ and note that $w_2 \in V_h$ since $b_h^0 \in \mathcal{P}_0(\mathcal{T}_h)$. Then

$$\begin{aligned} A_h(v, w_2) &= \|\phi_b^{1/2} b \cdot \nabla v\|_{\Omega}^2 + (b \cdot \nabla v, \phi_b (b_h^0 - b) \cdot \nabla v)_{\Omega} + (cv, w_2)_{\Omega} - (b \cdot nv, w_2)_{\Gamma-} \\ &\quad - (b \cdot n[v], \{w_2\})_{\mathcal{F}_h \cap \Omega} + \frac{1}{2} (|b \cdot n|[v], [w_2])_{\mathcal{F}_h \cap \Omega} + g_h(v, w_2) \end{aligned} \quad (5.20)$$

$$= \|\phi_b^{1/2} b \cdot \nabla v\|_{\Omega}^2 + I + II + III + IV + V + VI. \quad (5.21)$$

Term I can be bounded by successively applying a Cauchy-Schwarz inequality and (5.14),

$$|I| \leq \|\phi_b^{1/2} b \cdot \nabla v\|_{\Omega} \|\phi_b^{1/2} (b_h^0 - b) \cdot \nabla v\|_{\Omega} \lesssim \|\phi_b^{1/2} b \cdot \nabla v\|_{\Omega} \|v\|_{\text{up},h}. \quad (5.22)$$

To estimate the remaining terms $II-VI$, let us for the moment assume that the stability estimate

$$\|w_2\|_{\text{sd},h,*} \lesssim \|v\|_{\text{sd},h} \quad (5.23)$$

holds. Then one can easily see that

$$|II| + \dots + |VI| \lesssim \|v\|_{\text{up},h} \|w_2\|_{\text{sd},h,*} \lesssim \|v\|_{\text{up},h} \|v\|_{\text{sd},h}. \quad (5.24)$$

Combing (5.22) and (5.24), we can estimate the right-hand side of (5.21) further by employing a Young inequality of the form $ab \leq \delta a^2 + \frac{1}{4\delta} b^2$ yielding

$$A_h(v, w_2) \geq \|\phi_b^{1/2} b \cdot \nabla v\|_{\Omega}^2 - \|\phi_b^{1/2} b \cdot \nabla v\|_{\Omega} \|v\|_{\text{up},h} - C \|v\|_{\text{up},h} \|v\|_{\text{sd},h} \quad (5.25)$$

$$\geq \|\phi_b^{1/2} b \cdot \nabla v\|_{\Omega}^2 - \delta \|\phi_b^{1/2} b \cdot \nabla v\|_{\Omega} - \frac{1}{4\delta} \|v\|_{\text{up},h}^2 - \delta C \|v\|_{\text{sd},h}^2 - \frac{C}{4\delta} \|v\|_{\text{up},h}^2 \quad (5.26)$$

$$= (1 - \delta - \delta C) \|\phi_b^{1/2} b \cdot \nabla v\|_{\Omega}^2 - \left(\frac{1}{4\delta} + C\delta + \frac{C}{4\delta}\right) \|v\|_{\text{up},h}^2 \quad (5.27)$$

$$= \frac{1}{2} \|\phi_b^{1/2} b \cdot \nabla v\|_{\Omega}^2 - \frac{(1+C)^3 + C}{2(1+C)} \|v\|_{\text{up},h}^2, \quad (5.28)$$

for some constant C and $\delta = \frac{1}{2+2C}$. This gives us the desired control over the streamline derivative.

Step 3. To construct a suitable test function for given v , we set now $w_3 = w_1 + \delta c_0 \tau_c w_2$. Thanks to stability estimate (5.23) we have $\|w_3\|_{\text{sd},h} \lesssim \|v\|_{\text{sd},h} + \delta c_0 \tau_c \|v\|_{\text{sd},h} \leq (1 + \delta) \|v\|_{\text{sd},h}$ and thus combining (5.19) and (5.28) leads us to

$$\begin{aligned} A_h(v, w_3) &\geq (1 - \delta \tilde{C}) c_0 \tau_c \|v\|_{\text{up},h}^2 + \frac{\delta}{2} c_0 \tau_c \|\phi_b^{1/2} b \cdot \nabla v\|_{\Omega}^2 \\ &\gtrsim c_0 \tau_c \|v\|_{\text{sd},h}^2 \gtrsim c_0 \tau_c \|v\|_{\text{sd},h} \|w_3\|_{\text{sd},h} \end{aligned} \quad (5.29)$$

for some constant \tilde{C} and $\delta > 0$ small enough. Dividing by $\|w_3\|_{\text{sd},h}$ and taking the supremum over v proves (5.18). To complete the proof, it remains to establish the stability bound (5.23).

Estimate (5.23). We start by unwinding the definition of $\|\cdot\|_{\text{sd},h,*}$,

$$\|w_2\|_{\text{sd},h,*}^2 = \tau_c^{-1} \|w_2\|_{\Omega}^2 + \|\phi_b^{1/2} b \cdot \nabla w_2\|_{\Omega}^2 + \frac{1}{2} \|b \cdot n^{1/2} w_2\|_{\Gamma}^2 + b_c \|w_2\|_{\partial \mathcal{T}_h \cap \Omega}^2 + |w_2|_{g_h}^2 \quad (5.30)$$

$$= I + II + III + IV + V. \quad (5.31)$$

The main tool to estimate I – V is inequality (5.15) with $P = T$, $\mathcal{P}_h = \mathcal{T}_h$ and $b_h^P = b_h^0$. Inserting the definition of $w_2 = \phi_b b_h^0 \cdot \nabla v$ and the fact that $\phi_b \tau_c^{-1} \leq 1$ thanks to assumption (4.8) yields

$$I = \tau_c^{-1} \|\phi_b b_h^0 \cdot \nabla v\|_{\Omega}^2 = \tau_c^{-1} \phi_b \|\phi_b^{1/2} b_h^0 \cdot \nabla v\|_{\Omega}^2 \leq \|\phi_b^{1/2} b_h^0 \cdot \nabla v\|_{\Omega}^2 \lesssim \|v\|_{\text{sd},h}^2. \quad (5.32)$$

The second term II can be dealt with by recalling the definition of ϕ_b , applying the inverse estimate (4.12) and subsequently moving to the streamline diffusion norm via (5.15),

$$II = \|\phi_b^{1/2} b \cdot \nabla(\phi_b b_h^0 \cdot \nabla v)\|_{\Omega}^2 \lesssim b_c h \|\nabla(\phi_b b_h^0 \cdot \nabla v)\|_{\Omega}^2 \lesssim b_c h^{-1} \|\phi_b b_h^0 \cdot \nabla v\|_{\mathcal{T}_h}^2 \quad (5.33)$$

$$\lesssim \|\phi_b^{1/2} b_h^0 \cdot \nabla v\|_{\mathcal{T}_h}^2 \lesssim \|v\|_{\text{sd},h}^2. \quad (5.34)$$

Next, invoking the inverse trace estimates (4.14) followed by an application of (5.15), we see that

$$III \lesssim b_c \|\phi_b b_h^0 \cdot \nabla v\|_{\Gamma}^2 \lesssim \|(h \phi_b)^{1/2} b_h^0 \cdot \nabla v\|_{\Gamma}^2 \lesssim \|\phi_b^{1/2} b_h^0 \cdot \nabla v\|_{\mathcal{T}_h}^2 \lesssim \|v\|_{\text{sd},h}^2, \quad (5.35)$$

and similarly for IV ,

$$IV = b_c \|\phi_b b_h^0 \cdot \nabla v\|_{\partial \mathcal{T}_h \cap \Omega}^2 \lesssim \|\phi_b^{1/2} b_h^0 \cdot \nabla v\|_{\mathcal{T}_h}^2 \lesssim \|v\|_{\text{sd},h}^2. \quad (5.36)$$

After using (5.11), the remaining last term V can be estimated by proceeding as for I and II :

$$V = |w_2|_{g_c}^2 + |w_2|_{g_b}^2 \lesssim \tau_c^{-1} \|w_2\|_{\mathcal{T}_h}^2 + \|\phi_b^{1/2} b_h^0 \cdot \nabla w_2\|_{\mathcal{T}_h}^2 \lesssim \|v\|_{\text{sd},h}^2. \quad (5.37)$$

□

We conclude this section with a couple of remarks, elucidating the role of the ghost penalties g_c and g_b .

Remark 5.8. We point out that the most critical part in the derivation of the inf-sup condition (5.18) is the proof of the stability estimate (5.23). At several occasions it involves inverse estimates of the form (4.12)–(4.14) to pass from $w_2 = \phi_b b_h^0 \cdot \nabla v$ to v in the streamline diffusion norm. As a result, we need to control the streamline derivative of v on the *entire* active mesh \mathcal{T}_h , which is precisely the role of the ghost penalty g_b .

Remark 5.9. The role of the ghost penalty g_c twofold. In the previous proof, the ghost penalty g_c is only needed to pass between b and b_h^0 by controlling various norm expressions involving $b - b_h^0$ and v in terms of $\tau_c^{-1/2} \|v\|_{\mathcal{T}_h}$. Consequently, the ghost penalty g_c could have been omitted if $b \in \mathbb{P}_1(\mathcal{T}_h)$ since then $\phi_b b \cdot \nabla v \in V_h$. Nevertheless, we will see that g_c is indeed needed to ensure that the condition number of the system matrix is robust with respect to the boundary position relative to the background mesh, see Section 7.

Remark 5.10. The previous derivation rises the question whether the ghost penalty g_b is only needed because of the use of the stronger norm $||| \cdot |||_{\text{sd}}$ instead of the more classical $||| \cdot |||_{\text{up}}$ norm. A closer look at the numerical analysis based on the $||| \cdot |||_{\text{up}}$ norm as presented in [62] reveals that g_b cannot be avoided. The reason is that the a priori analysis based on $||| \cdot |||_{\text{up}}$ exploits the orthogonality of the L^2 projection operator π_h to rewrite the advection related term in (5.1) to

$$(\pi_h u - u, b \cdot \nabla v)_\Omega = (\pi_h u - u, (b - b_h^0) \cdot \nabla v)_\Omega \quad (5.38)$$

to arrive at an optimal error estimate for the advection related error terms in the $|||u - u_h|||_{\text{up}}$ norm. In the unfitted case though, it is not possible to define a *stable* orthogonal projection operator using the L^2 scalar product $(\cdot, \cdot)_\Omega$ considering only the physical domain Ω . The orthogonality of the unfitted L^2 projection π_h^e constructed in Section 4 is perturbed as it satisfies only $(\pi_h^e u - u^e, v)_{\mathcal{T}_h} = 0$ for $v \in V_h$. Therefore, we get now

$$(\pi_h^e u - u^e, b \cdot \nabla v)_\Omega = (\pi_h^e u - u^e, (b - b_h) \cdot \nabla v)_\Omega - (\pi_h u^e - u^e, b_h \cdot \nabla v)_{\mathcal{T}_h \setminus \Omega}, \quad (5.39)$$

and thus we need to provide sufficient control of $\|\phi_b^{1/2} b_h \cdot \nabla v\|_{\mathcal{T}_h \setminus \Omega}$ in the relevant norms to handle the second term in (5.39).

6. A priori error analysis

We turn to the a priori error analysis of the unfitted discretization scheme (3.9). To keep the technical details at a moderate level, we assume for a priori error analysis that the contributions from the cut elements $\mathcal{T}_h \cap \Omega$, the cut faces $\mathcal{F}_h \cap \Omega$ and the boundary parts $\Gamma \cap \mathcal{T}_h$ can be computed exactly. For a thorough treatment of variational crimes arising from the discretization of a curved boundary, we refer the reader to [82–84]. We start with quantifying the effect of the stabilization g_h on the consistency of the total bilinear form A_h defined by (3.9).

Lemma 6.1 (Weak Galerkin orthogonality). *Let $u \in H^1(\Omega)$ be the solution ² to (2.1) and let u_h be the solution to the discrete formulation (3.9). Then*

$$a_h(u - u_h, v) - g_h(u_h, v) = 0 \quad (6.1)$$

PROOF. The proof is a direct consequence of the fact that u satisfies $a_h(u, v) = l_h(v) \forall v \in V_h$. \square

²We assume $u \in H^1(\Omega)$ to simplify the presentation, but weaker regularity assumptions can be made, see for instance [68].

Theorem 6.2 (A priori error estimate). For $s \geq 2$, let $u \in H^s(\Omega)$ be the solution to the advection-reaction problem (2.1) and let u_h be the solution to the stabilized cutDG formulation (3.9). Then with $r = \min\{s, p+1\}$ it holds that

$$\|u - u_h\|_{\text{sd}} \lesssim (c_0 \tau_c)^{-1} b_c^{1/2} h^{r-1/2} \|u\|_{r, \Omega}. \quad (6.2)$$

PROOF. Decompose $u - u_h$ into an projection error $e_\pi = u - \pi_h u$ and a discrete error $e_h = \pi_h u - u_h$. Thanks to the interpolation estimate (4.24), it is enough to estimate the discrete error e_h for which the inf-sup condition (5.18) implies that

$$c_0 \tau_c \|e_h\|_{\text{sd}, h} \lesssim \sup_{v \in V_h \setminus \{0\}} \frac{A_h(e_h, v)}{\|v\|_{\text{sd}, h}} \quad (6.3)$$

$$= \sup_{v \in V_h \setminus \{0\}} \frac{a_h(e_\pi, v) + g_h(\pi_h u, v)}{\|v\|_{\text{sd}, h}} \quad (6.4)$$

$$\lesssim \sup_{v \in V_h \setminus \{0\}} \frac{\|e_\pi\|_{\text{sd}, *}\|v\|_{\text{up}} + |\pi_h u|_{g_h}|v|_{g_h}}{\|v\|_{\text{sd}, h}} \quad (6.5)$$

$$\lesssim \|e_\pi\|_{\text{sd}, *} + |\pi_h u|_{g_h}. \quad (6.6)$$

Recalling assumption (4.8) and its reformulation (4.9), the bounds for the consistency and approximation error stated in Assumption HP1 and Eq.(4.24) show that

$$\|u - u_h\|_{\text{sd}} \lesssim \|e_\pi\|_{\text{sd}} + \|e_h\|_{\text{sd}, h} \lesssim (c_0 \tau_c)^{-1} (\|e_\pi\|_{\text{sd}, *} + |\pi_h u|_{g_h}) \quad (6.7)$$

$$\lesssim (c_0 \tau_c)^{-1} (\tau_c^{1/2} h^{1/2} + b_c^{1/2}) h^{r-1/2} \|u\|_{r, \Omega} \lesssim (c_0 \tau_c)^{-1} b_c^{1/2} h^{r-1/2} \|u\|_{r, \Omega}, \quad (6.8)$$

which concludes the proof. \square

7. Condition number estimates

We now conclude the numerical analysis of the cutDG method for the advection-reaction problem by showing that the condition number associated with bilinear form (3.9) can be bounded by Ch^{-1} with a constant independent of particular cut configuration. Our derivation is inspired by the presentation in [85].

Let $\{\phi_i\}_{i=1}^N$ be the standard piecewise polynomial basis functions associated with $V_h = \mathbb{P}_p(\mathcal{T}_h)$ so that any $v \in V_h$ can be written as $v = \sum_{i=1}^N V_i \phi_i$ with coefficients $V = \{V_i\}_{i=1}^N \in \mathbb{R}^N$. The system matrix \mathcal{A} associated with A_h is defined by the relation

$$(\mathcal{A}V, W)_{\mathbb{R}^N} = A_h(v, w) \quad \forall v, w \in V_h. \quad (7.1)$$

Thanks to the L^2 coercivity of A_h , the system matrix \mathcal{A} is a bijective linear mapping $\mathcal{A} : \mathbb{R}^N \rightarrow \mathbb{R}^N$ with its operator norm and condition number defined by

$$\|\mathcal{A}\|_{\mathbb{R}^N} = \sup_{V \in \mathbb{R}^N \setminus \{0\}} \frac{\|\mathcal{A}V\|_{\mathbb{R}^N}}{\|V\|_{\mathbb{R}^N}} \quad \text{and} \quad \kappa(\mathcal{A}) = \|\mathcal{A}\|_{\mathbb{R}^N} \|\mathcal{A}^{-1}\|_{\mathbb{R}^N}, \quad (7.2)$$

respectively. To pass between the discrete l^2 norm of coefficient vectors V and the continuous L^2 norm of finite element functions v_h , we need to recall the well-known estimate

$$h^{d/2} \|V\|_{\mathbb{R}^N} \lesssim \|v\|_{L^2(\mathcal{T}_h)} \lesssim h^{d/2} \|V\|_{\mathbb{R}^N}, \quad (7.3)$$

which holds for any quasi-uniform mesh \mathcal{T}_h and $v \in V_h$. Then we can prove the following theorem.

Theorem 7.1. The condition number of the system matrix \mathcal{A} associated with (3.9) satisfies

$$\kappa(\mathcal{A}) \lesssim b_c (c_0 h)^{-1} \quad (7.4)$$

independent of how the boundary Γ cuts the background mesh \mathcal{T}_h .

PROOF. The definition of the condition number requires to bound $\|\mathcal{A}\|_{\mathbb{R}^N}$ and $\|\mathcal{A}^{-1}\|_{\mathbb{R}^N}$.

Estimate of $\|\mathcal{A}\|_{\mathbb{R}^N}$. We start by estimating $A_h(v, w) = a_h(v, w) + g_h(v, w) \forall v, w \in V_h$. To bound the first term a_h , successively employ a Cauchy-Schwarz inequality and the inverse trace inequalities (4.13) and (4.14) to obtain

$$a_h(v, w) \lesssim \|c\|_{0,\infty,\Omega} \|v\|_{\Omega} \|w\|_{\Omega} + \|b \cdot \nabla v\|_{\Omega} \|w\|_{\Omega} + \| |b \cdot n|^{1/2} v \|_{\Gamma} \| |b \cdot n|^{1/2} w \|_{\Gamma} \quad (7.5)$$

$$+ \| |b \cdot n|^{1/2} v \|_{\mathcal{F}_h \cap \Omega} \| |b \cdot n|^{1/2} w \|_{\mathcal{F}_h \cap \Omega} \quad (7.6)$$

$$\lesssim \|c\|_{0,\infty,\Omega} \|v\|_{\Omega} \|w\|_{\Omega} + h^{-1} b_c \|v\|_{\mathcal{T}_h} \|w\|_{\mathcal{T}_h} \lesssim h^{-1} b_c \|v\|_{\mathcal{T}_h} \|w\|_{\mathcal{T}_h}, \quad (7.7)$$

where we used (4.9) in the last step. Next, note that by assumption (5.11), we have that

$$|v|_{g_h}^2 \lesssim \|b \cdot \nabla v\|_{\mathcal{T}_h}^2 + \tau_c^{-1} \|v\|_{\mathcal{T}_h}^2 \lesssim b_c h^{-1} \|v\|_{\mathcal{T}_h}^2, \quad (7.8)$$

and thus

$$g_h(v, w) \lesssim |v|_{g_h} |w|_{g_h} \lesssim b_c h^{-1} \|v\|_{\mathcal{T}_h} \|w\|_{\mathcal{T}_h}. \quad (7.9)$$

As a result of these estimates and (7.3), we have

$$A_h(v, w) \lesssim b_c h^{-1} \|v\|_{\mathcal{T}_h} \|w\|_{\mathcal{T}_h} \lesssim b_c h^{d-1} \|V\|_{\mathbb{R}^N} \|W\|_{\mathbb{R}^N}, \quad (7.10)$$

which allows us to estimate $\|\mathcal{A}\|_{\mathbb{R}^N}$ by

$$\|\mathcal{A}\|_{\mathbb{R}^N} = \sup_{V \in \mathbb{R}^N \setminus \{0\}} \sup_{W \in \mathbb{R}^N \setminus \{0\}} \frac{(\mathcal{A}V, W)_{\mathbb{R}^N}}{\|V\|_{\mathbb{R}^N} \|W\|_{\mathbb{R}^N}} \quad (7.11)$$

$$= \sup_{V \in \mathbb{R}^N \setminus \{0\}} \sup_{W \in \mathbb{R}^N \setminus \{0\}} \frac{A_h(v, w)}{\|V\|_{\mathbb{R}^N} \|W\|_{\mathbb{R}^N}} \lesssim b_c h^{d-1}. \quad (7.12)$$

Estimate of $\|\mathcal{A}^{-1}\|_{\mathbb{R}^N}$. The discrete coercivity result (5.6) and assumption (5.10) implies that

$$A_h(v, v) \gtrsim c_0 \tau_c \|v\|_{\text{up},h}^2 \gtrsim c_0 \|v\|_{\mathcal{T}_h}^2 \gtrsim c_0 h^d \|V\|_{\mathbb{R}^N}^2, \quad (7.13)$$

and as a result,

$$\|\mathcal{A}V\|_{\mathbb{R}^N} = \sup_{W \in \mathbb{R}^N \setminus \{0\}} \frac{(\mathcal{A}V, W)_{\mathbb{R}^N}}{\|W\|_{\mathbb{R}^N}} \geq \frac{(AV, V)_{\mathbb{R}^N}}{\|V\|_{\mathbb{R}^N}} = \frac{A_h(v, v)}{\|V\|_{\mathbb{R}^N}} \gtrsim c_0 h^d \|V\|_{\mathbb{R}^N}. \quad (7.14)$$

Setting $V = \mathcal{A}^{-1}W$, the previous chain of estimates shows that $\|\mathcal{A}^{-1}\|_{\mathbb{R}^N} \lesssim c_0^{-1} h^{-d}$ which in combination with (7.12) gives the desired bound

$$\|\mathcal{A}\|_{\mathbb{R}^N} \|\mathcal{A}^{-1}\|_{\mathbb{R}^N} \lesssim b_c (c_0 h)^{-1}. \quad (7.15)$$

□

8. Ghost penalty realizations

In this section we present a number of possible realizations of the ghost penalty operators satisfying our Assumptions HP1, HP2, and HP3. We briefly discuss the L^2 norm related ghost penalty g_c first and then derive corresponding realizations of g_b . So far, three construction principles exist in the literature. The first one is the classical *face-based* ghost penalty proposed by [86] for continuous \mathbb{P}_1 elements. High-order variants were then introduced in Burman [87], for a detailed analysis we refer to [87, 88]. In face-based ghost penalties, jumps of normal-derivatives of all relevant polynomial orders across faces belonging to the face set

$$\mathcal{F}_h^g = \{F \in \mathcal{F}_h : T^+ \cap \Gamma \neq \emptyset \vee T^- \cap \Gamma \neq \emptyset\} \quad (8.1)$$

are penalized. For our current problem class, the corresponding dG variant extending the L^2 norm is given by

$$g_c^f(v, w) = \gamma_c^f c_0 \sum_{j=0}^p h^{2j+1} ([\partial_n^j v], [\partial_n^j w])_{\mathcal{F}_h^g}, \quad (8.2)$$

where the notation $\partial_n^j v := \sum_{|\alpha|=j} \frac{D^\alpha v(x) n^\alpha}{\alpha!}$ for multi-indices $\alpha = (\alpha_1, \dots, \alpha_d)$, $|\alpha| = \sum_i \alpha_i$ and $n^\alpha = n_1^{\alpha_1} n_2^{\alpha_2} \dots n_d^{\alpha_d}$ is used. The constant γ_c^f denotes a dimensionless stability parameter.

In [87] and later in [23], alternative ghost penalties were proposed which were based on a *local projection stabilization*. For a given patch P of $\text{diam}(P) \lesssim h$ containing the two elements T_1 and T_2 , one defines the L^2 projection $\pi_P : L^2(P) \rightarrow \mathbb{P}_p(P)$ onto the space of polynomials of order p associated with the patch P . For $v \in V_h$, the fluctuation operator $\kappa_P = \text{Id} - \pi_P$ measures then the deviation of $v|_P$ from being a polynomial defined on P . By choosing certain patch definitions, a coupling between elements with a possible small cut and those with a fat intersection is ensured. One patch choice arises naturally from the definition of \mathcal{F}_h^g by defining the patch $P(F) = T_F^+ \cup T_F^-$ for two elements T_F^+, T_F^- sharing the interior face F and setting

$$\mathcal{P}_1 = \{P(F)\}_{F \in \mathcal{F}_h^g}. \quad (8.3)$$

A second possibility is to use neighborhood patches $\omega(T)$,

$$\mathcal{P}_2 = \{\omega(T)\}_{T \in \mathcal{T}_\Gamma}. \quad (8.4)$$

Finally, one can mimic the cell agglomeration approach taken in classical unfitted discontinuous Galerkin approaches [43, 46, 47, 55] by associating to each cut element $T \in \mathcal{T}_\Gamma$ with a small intersection $|T \cap \Omega|_d \ll |T|_d$ an element $T' \in \omega(T)$ satisfying the fat intersection property $|T' \cap \Omega|_d \geq c_s |T'|^d$. Introducing the “agglomerated patch” $P_a(T) = T \cup T'$, a proper collection of patches is given by

$$\mathcal{P}_3 = \{P_a(T) \mid T \in \mathcal{T}_\Gamma \wedge |T \cap \Omega|_d \leq c_s |T|_d\}. \quad (8.5)$$

The resulting *local projection* based ghost penalty extending the L^2 norm in the sense of HP2 are then defined as follows:

$$g_c^p(v, w) = \gamma_c^p c_0 \sum_{P \in \mathcal{P}} (\kappa_P v, \kappa_P w)_P, \quad \mathcal{P} \in \{\mathcal{P}_1, \mathcal{P}_2, \mathcal{P}_3\}. \quad (8.6)$$

Finally, an elegant version of a patch-based ghost penalty avoiding the assembly of local projection matrices completely was recently proposed in [89]. Using the natural global polynomial extension u_i^e every polynomial u_i on an element T_i possesses, a volume-based jump on a patch $P = T_1 \cup T_2$ can be defined by $[u]_P = u_1^e - u_2^e$ which give raise to the *volume based* ghost penalty

$$g_c^v(v, w) = \gamma_b^v c_0 \sum_{P \in \mathcal{P}_1} ([v]_P, [w]_P)_P, \quad \mathcal{P} \in \{\mathcal{P}_1, \mathcal{P}_3\}. \quad (8.7)$$

Lemma 8.1. *Each of the face, projection and volume-based realizations of g_c satisfies Assumptions HP1 and HP2.*

PROOF. As the original proofs require only minimal adaption to derive HP1 and HP2 for discontinuous ansatz functions instead of continuous ones, we refer to [87] and [88] for the analysis of g_h^p and g_h^f , and to [89] for the volume penalty g_h^v .

Next, we design proper realization of the advection related ghost penalty g_b . The natural idea is to start from g_c and to replace v with $\phi_b^{1/2} b \cdot \nabla v$ as we wish to control the L^2 norm of the scaled streamline derivative. This idea leads us to the following lemma.

Lemma 8.2. *Each of the face, projection and volume-based realizations of g_b defined by*

$$g_b^f(v, w) = \gamma_b^f \sum_{j=0}^p \phi_b h^{2j+1} ([b_h^P \cdot \nabla \partial_n^j v], [b_h^P \cdot \nabla \partial_n^j w])_{\mathcal{F}_h^g}, \quad (8.8)$$

$$g_b^p(v, w) = \gamma_b^p \sum_{P \in \mathcal{P}} \phi_b (\kappa_P(b_h^P \cdot \nabla v), \kappa_P(b_h^P \cdot \nabla w))_P, \quad \mathcal{P} \in \{\mathcal{P}_1, \mathcal{P}_2, \mathcal{P}_3\}, \quad (8.9)$$

$$g_b^v(v, w) = \gamma_b^v \sum_{P \in \mathcal{P}_1} \phi_b ([b_h^P \cdot \nabla v]_P, [b_h^P \cdot \nabla w]_P)_P, \quad \mathcal{P} \in \{\mathcal{P}_1, \mathcal{P}_3\} \quad (8.10)$$

satisfies Assumption [HP1](#) and [HP3](#). Here, we choose b_h^P to be a patch-wise defined, constant vector-valued function satisfying the assumptions of Lemma [5.4](#). For g_b^f , the vector field b_h^P is understood to be defined on each face patch $P(F) = T_F^+ \cup T_F^-$.

PROOF. Here, we consider only g_b^v as the analysis for g_b^p and g_b^f is rather similar, and a detailed theoretical analysis of the g_b^f can be also found in [\[27\]](#).

We start with the verification of Assumption [HP3](#). First recall, that for two incident elements T_1 and T_2 and $P = T_1 \cup T_2$, the norm equivalence $\|w\|_{T_1}^2 \sim \|w\|_{T_2}^2 + \|[w]_P\|_P^2$ holds for $w \in V_h$. Setting $w = \phi_b^{1/2} b_h^P \cdot \nabla v$ and using Lemma [5.4](#), Eq.([5.14](#)), to pass between $\phi_b^{1/2} b_h^P \cdot \nabla v$ and $\phi_b^{1/2} b \cdot \nabla v$, we conclude that

$$\|\phi_b^{1/2} b \cdot \nabla v\|_{T_1}^2 \lesssim \|\phi_b^{1/2} b_h^P \cdot \nabla v\|_{T_1}^2 + \|\phi_b^{1/2} (b_h^P - b) \cdot \nabla v\|_{T_1}^2 \quad (8.11)$$

$$\lesssim \|\phi_b^{1/2} b_h^P \cdot \nabla v\|_{T_1}^2 + \tau_c^{-1} \|v\|_{T_1}^2 \quad (8.12)$$

$$\lesssim \|\phi_b^{1/2} b_h^P \cdot \nabla v\|_{T_2}^2 + \|[\phi_b^{1/2} b_h^P \cdot \nabla v]_P\|_P^2 + \tau_c^{-1} \|v\|_{T_1}^2 \quad (8.13)$$

$$\lesssim \|\phi_b^{1/2} b \cdot \nabla v\|_{T_2}^2 + \tau_c^{-1} \|v\|_{T_2}^2 + \|[\phi_b^{1/2} b_h^P \cdot \nabla v]_P\|_P^2 + \tau_c^{-1} \|v\|_{T_1}^2. \quad (8.14)$$

This together with the geometric assumption [G2](#) and the norm equivalence $\|\phi_b^{1/2} b \cdot \nabla v\|_{T_2}^2 \sim \|\phi_b^{1/2} b \cdot \nabla v\|_{T_2 \cap \Omega}^2$ on elements T_2 with a fat intersection implies that

$$\|\phi_b^{1/2} b \cdot \nabla v\|_{\mathcal{T}_h}^2 \lesssim \|\phi_b^{1/2} b \cdot \nabla v\|_{\Omega}^2 + |v|_{g_b^v}^2 + \tau_c^{-1} \|v\|_{\Omega}^2 + |v|_{g_c}^2, \quad (8.15)$$

proving the first inequality in Assumption [HP3](#). The second inequality easily follows from assumption [HP3](#) implying that $|v|_{g_c}^2 \lesssim \tau_c^{-1} \|v\|_{\mathcal{T}_h}^2$ and the fact that $|v|_{g_b^v}^2 \lesssim \|\phi_b^{1/2} b \cdot \nabla v\|_P^2 + \tau_c^{-1} \|v\|_P^2$.

To prove the weak consistency assumption [HP1](#), simply observe that $[\phi_b^{1/2} b_h^P \cdot \nabla \pi_P u^e]_P = 0$ for $u \in H^s(\Omega)$, $s \geq 1$, and the patch-wise defined L^2 projection π_P , and thus

$$\sum_{P \in \mathcal{P}} \|[\phi_b^{1/2} b_h^P \cdot \nabla \pi_h^e u]\|_P^2 = \sum_{P \in \mathcal{P}} \|[\phi_b^{1/2} b_h^P \cdot \nabla (\pi_h^e u - \pi_P u^e)]\|_P^2 \quad (8.16)$$

$$\lesssim \sum_{P \in \mathcal{P}} \|\phi_b^{1/2} b_h^P \cdot \nabla (\pi_h^e u - u^e)\|_P^2 + \sum_{P \in \mathcal{P}} \|\phi_b^{1/2} b_h^P \cdot \nabla (u - \pi_P u^e)\|_P^2 \quad (8.17)$$

$$\lesssim \phi_b b_c^2 h^{2(r-1)} \|u^e\|_{r, \mathcal{T}_h}^2 \lesssim b_c h^{2r-1} \|u\|_{r, \Omega}^2. \quad (8.18)$$

which concludes the proof. \square

Remark 8.3. It is possible to replace the convection and reaction related stabilization forms g_b and g_c by a unified ghost penalty. For instance, for the face-based realizations [\(8.2\)](#) and [\(8.8\)](#) operator a single ghost penalty of the form

$$g^f(v, w) = \gamma^f \sum_{j=0}^p \left(c_0 + \frac{b_c}{h}\right) h^{2j+1} ([\partial_n^j v], [\partial_n^j w])_{\mathcal{F}_h^g}, \quad (8.19)$$

can be used instead, at the cost of introducing some additional (order-preserving) cross-wind diffusion. Consequently, only face jump penalties of the form $[\partial_n^j(\cdot)]$ need to be implemented. We refer to [\[27\]](#)[Remark 3.4] for a detailed discussion.

9. Numerical results

This section is devoted to a number of numerical experiments supporting our theoretical findings. First, convergence rate studies for smooth manufactured solutions defined on complex 2D and 3D domains are presented. In a second convergence study, we also consider both higher order elements and rough solutions with a internal sharp layer in the domain. We conclude this section with two numerical studies illustrating the importance of the ghost penalties for the geometrical robustness of the derived a priori error and condition number estimates.

9.1. Convergence rate experiments

In the first series of experiments, we will test the convergence of the proposed cutDG over various geometries, dimensions, and polynomial orders. Common to all examples below, a background mesh $\tilde{\mathcal{T}}_0$ for the embedding domain $\Omega_0 = [-a, a]^d$ is created and successively refined, from which the active background meshes $\{\mathcal{T}_k\}_{k=0}^N$ are extracted. The mesh size is then given by $h_k = 2a \cdot 2^{-3-k}$. For a given polynomial order p and active mesh \mathcal{T}_k , we compute the numerical solution $u_k^p \in \mathbb{P}_p(\mathcal{T}_k)$ from (3.9) using the ghost penalties defined in (8.8) and (8.2). The experimental order of convergence (EOC) shown in convergence tables is calculated by using

$$\text{EOC}(k, p) = \frac{\log(E_{k-1}^p/E_k^p)}{\log(h_{k-1}/h_k)},$$

where $E_k^p = \|e_k^p\| = \|u - u_k^p\|$ denotes the error of the numerical approximation u_k^p measured in a certain norm $\|\cdot\|$. The error norms considered in our tests are the L^2 norm $\|\cdot\|_\Omega$, the upwind flux semi-norm $\frac{1}{2}\|b \cdot n|^{1/2}[\cdot]\|_{\mathcal{F}_h}$ and the streamline diffusion semi-norm $\|\phi^{1/2}b \cdot \nabla(\cdot)\|_\Omega$; in accordance with the a priori error estimates presented in Section 5.

9.1.1. Flower and popcorn domains

To demonstrate the capability of the presented cutDGM to treat complex geometries in different dimensions, we consider two test cases.. In our first test case, we numerically solve the hyperbolic equation (2.1) over a two dimensional flower domain that is defined by

$$\Omega = \{(x, y) \in \mathbb{R}^2 \mid \phi(x, y) < 0\} \quad \text{with } \Phi(x, y) = \sqrt{x^2 + y^2} - r_0 - r_1 \cos(5 \operatorname{atan}_2(y, x)), \quad (9.1)$$

with $r_0 = 0.5$ and $r_1 = 0.15$, see Figure 9.1 (left). The manufactured solution u , the vector velocity field b , and reaction term c are taken from [90] and given by

$$u(x, y) = 1 + \sin(\pi(1+x)(1+y)^2/8), \quad b(x, y) = (0.8, 0.6), \quad c = 1.0. \quad (9.2)$$

For the three-dimensional test case, the domain of interest is a popcorn like geometry defined by

$$\Phi(x, y, z) = \sqrt{x^2 + y^2 + z^2} - r_0 - \sum_{k=0}^{11} A \exp(-(x - x_k)^2 + (y - y_k)^2 + (z - z_k)^2)/\sigma^2,$$

where

$$\begin{aligned} (x_k, y_k, z_k) &= \frac{r_0}{\sqrt{5}} \left(2 \cos\left(\frac{2k\pi}{5}\right), 2 \sin\left(\frac{2k\pi}{5}\right), 1 \right), \quad 0 \leq k \leq 4, \\ (x_k, y_k, z_k) &= \frac{r_0}{\sqrt{5}} \left(2 \cos\left(\frac{(2(k-5)-1)\pi}{5}\right), 2 \sin\left(\frac{(2(k-5)-1)\pi}{5}\right), -1 \right), \quad 5 \leq k \leq 9, \\ (x_k, y_k, z_k) &= (0, 0, r_0), \quad k = 10, \\ (x_k, y_k, z_k) &= (0, 0, -r_0), \quad k = 11, \end{aligned} \quad (9.3)$$

and

$$r_0 = 0.6, \sigma = 0.2, A = 2,$$

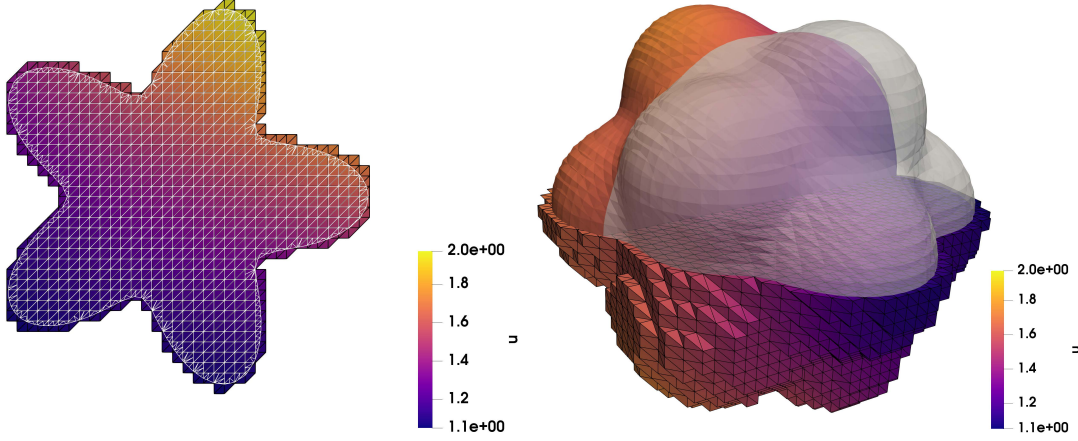


Figure 9.1: Solution plots for two dimensional flower (left) and three dimensional popcorn (right) examples. In both cases the solution is plotted over active background mesh \mathcal{T} , the domain boundary -in 2D- or surface -in 3D- and the physical domains are as well shown.

see Figure 9.1 (right). This time, we set the manufactured solution u , and the vector velocity field b , and the reaction term c to

$$u(x, y, z) = 1 + \sin(\pi(1+x)(1+y^2)(1+z^3)/8), \quad b(x, y, z) = (0.8, 0.6, 0.4), \quad c = 1.0. \quad (9.4)$$

For both examples we employ linear elements together with stabilization parameters $\gamma_0 = \gamma_1 = \beta_0 = 0.01$. The calculated EOCs are summarized in Table 9.1 and confirm the theoretically expected convergence rates of $\mathcal{O}(h^{3/2})$. For the L^2 norm, we even observe second-order convergence for these particular examples and mesh definitions, but we point out that this cannot be expected in general, see [91, 92].

Level N	$\ e_k\ _\Omega$	EOC	$\frac{1}{2} \ b \cdot n ^{1/2} [e_k] \ _{\mathcal{F}_h}$	EOC	$\ \phi^{1/2} b \cdot \nabla e_k\ _\Omega$	EOC
0	$8.58 \cdot 10^{-3}$	—	$1.17 \cdot 10^{-2}$	—	$2.21 \cdot 10^{-2}$	—
1	$1.98 \cdot 10^{-3}$	2.11	$3.91 \cdot 10^{-3}$	1.58	$5.14 \cdot 10^{-3}$	2.11
2	$5.05 \cdot 10^{-4}$	1.97	$1.30 \cdot 10^{-3}$	1.59	$1.70 \cdot 10^{-3}$	1.59
3	$1.30 \cdot 10^{-4}$	1.96	$4.44 \cdot 10^{-4}$	1.55	$5.86 \cdot 10^{-4}$	1.54
4	$3.23 \cdot 10^{-5}$	2.01	$1.56 \cdot 10^{-4}$	1.51	$2.12 \cdot 10^{-4}$	1.46

Level N	$\ e_k\ _\Omega$	EOC	$\frac{1}{2} \ b \cdot n ^{1/2} [e_k] \ _{\mathcal{F}_h}$	EOC	$\ \phi^{1/2} b \cdot \nabla e_k\ _\Omega$	EOC
0	$3.70 \cdot 10^{-2}$	—	$1.82 \cdot 10^{-2}$	—	$3.39 \cdot 10^{-2}$	—
1	$8.89 \cdot 10^{-3}$	2.06	$7.35 \cdot 10^{-3}$	1.31	$1.08 \cdot 10^{-2}$	1.65
2	$2.15 \cdot 10^{-3}$	2.05	$2.58 \cdot 10^{-3}$	1.51	$3.26 \cdot 10^{-3}$	1.73
3	$5.32 \cdot 10^{-4}$	2.02	$8.29 \cdot 10^{-4}$	1.64	$1.06 \cdot 10^{-3}$	1.63
4	$1.32 \cdot 10^{-4}$	2.01	$2.73 \cdot 10^{-4}$	1.60	$3.47 \cdot 10^{-4}$	1.61

Table 9.1: Convergence rates for the 2D flower example (top) and the 3D popcorn example (bottom) using $\mathbb{P}_1(\mathcal{T}_k)$.

9.1.2. Wavy inflow and outflow boundary

Next, we study the performance of the proposed cutDGM for high order elements and at the presence of a sharp internal layer in the manufactured solution. For the first test case, a smooth solution without a sharp internal layer is manufactured. For the second test case, only linear

elements are considered. In both test cases, the problem (2.1) is solved on the domain

$$\Omega = [-1.0, 1.0]^2 \cap \{\phi^+ < 0.85\} \cap \{\phi^- > -0.85\} \quad (9.5)$$

where

$$\phi^+(x, y) = y - 0.1 \cos(8x), \quad \phi^-(x, y) = y + 0.1 \cos(8x). \quad (9.6)$$

This time, the vector velocity field b and the analytical solution u are set to

$$\begin{aligned} u(x, y) &= \exp(\lambda(x, y) \arcsin((1 - x^2)\pi \cos(2\pi y)/25)) \arctan(\lambda(x, y)/\epsilon), \\ b(x, y) &= ((1 - x^2)\pi \cos(2\pi y)/25, (1 + 4x^2)/5), \end{aligned} \quad (9.7)$$

where $\lambda(x, y) = (x - 0.1 \sin(2\pi y))/5$. It is important to note that the manufactured solution u leads to a smooth function when $\epsilon = 1.0$, and to solution with a sharp internal layer when ϵ is set to a very small value. In the latter case, the manufactured solution is practically discontinuous whenever the internal layer cannot be resolved by the mesh. It is also important to realize that λ defines the shape of the internal layer. Thanks to the definition of the velocity field b , we observe that the inflow and outflow boundaries are defined by the level sets

$$\Gamma^- = \{\phi^- = -0.85\} \cap \Omega, \quad \Gamma^+ = \{\phi^+ = 0.85\} \cap \Omega, \quad (9.8)$$

see Figure 9.2. For our convergence tests, we study two extreme cases where we set $\epsilon = 1.0$ first and $\epsilon = 10^{-8}$ later. Recalling the a priori error analysis from Sections 5, the expected convergence rate for smooth solutions is $\mathcal{O}(h^{p+1/2})$. For the discontinuous case, one can only expect a convergence order of at most $\mathcal{O}(h^{1/2})$ in the (global) L^2 norm, independent of the chosen polynomial order p . Consequently, we consider only the case $p = 1$ for the nearly discontinuous solution.

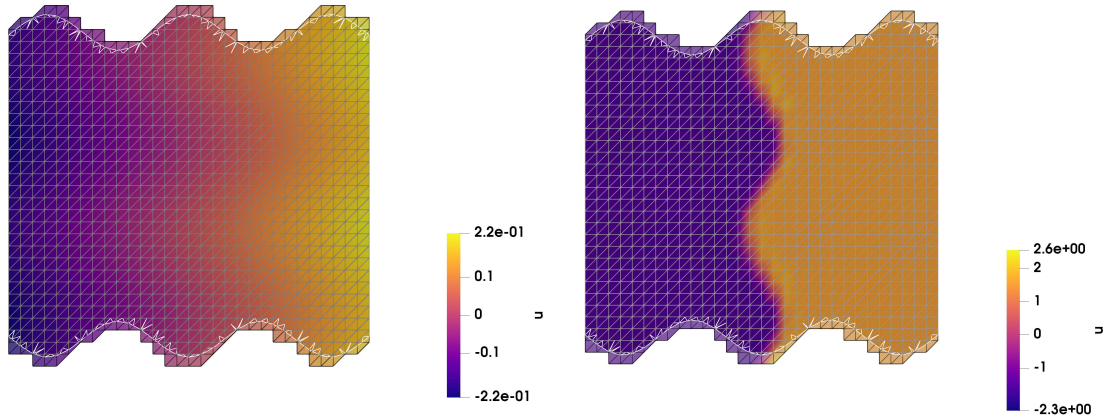


Figure 9.2: Solution plots for wavy inflow and outflow boundary example. Smooth solution with $\epsilon = 1$ (left) and the nearly discontinuous solution with $\epsilon = 10^{-8}$ (right). In both cases the solution is plotted over the active background mesh \mathcal{T}_k , the wavy inflow and outflow boundaries together with physical domain are shown as well.

a) Smooth case for $\epsilon = 1$ and high order

Setting $\epsilon = 1$ in (9.7), we obtain a smooth solution see Figure 9.2 (left). Employing high order elements up to $p = 3$, optimal convergence rates are obtained, see Figure 9.3. As before, we observe an EOC of $\mathcal{O}(h^{p+1})$ rather than $\mathcal{O}(h^{p+1/2})$ in the L^2 norm.

b) Discontinuous case for $\epsilon = 10^{-8}$

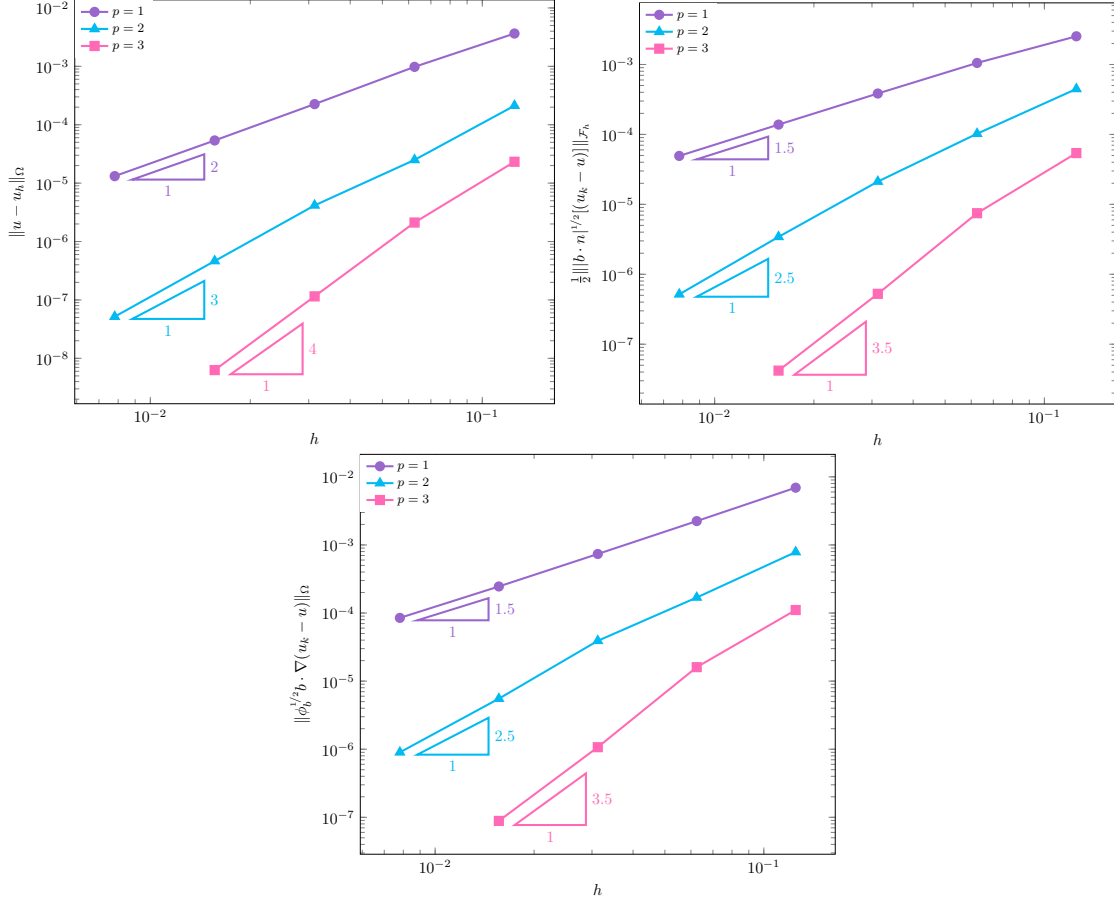


Figure 9.3: L^2 (top/left), upwind flux (top/right) and streamline diffusion (bottom) error convergence rates for wavy inflow and outflow example with $p = 1, 2, 3$. For $p = 3$, computer memory restrictions allowed us only to perform three mesh refinements instead of 4.

Next, we set $\epsilon = 10^{-8}$ in (9.7), where we observe a sharp internal layer in the middle of the domain, see Figure 9.2 (right). For our mesh resolution, this layer can be considered as discontinuous and the tabulated results in Table 9.2 confirm the reduction of the convergence order to $\mathcal{O}(h^{1/2})$ in the L^2 norm, and no convergence in the other considered error norms.

9.2. Geometrical robustness

In a final series of experiments, we numerically investigate the geometrical robustness of the derived a priori error and condition number estimates, illustrating the importance and different roles of the ghost penalties g_c and g_b . Our experiments are based on the following setup. We start from a structured background mesh $\tilde{\mathcal{T}}_h$ for the rectangular domain $\tilde{\Omega} = [-0.35, 0.35]^2 \subset \mathbb{R}^2$ with mesh size $h = 0.7/N$ and $N = 10$. To generate potentially critical cut configurations, we define a family $\{\Omega_{\delta_k}\}_{k=1}^{1000}$ of translated circular domains $\Omega_{\delta_k} = \Omega + \delta_k \mathbf{t}$ with the the initial domain $\Omega = \{(x, y) \in \mathbb{R}^2 \mid x^2 + y^2 - 0.25^2 < 0\}$ and set the translation vector \mathbf{t} and translation parameter δ_k to $\frac{1}{\sqrt{2}}(h, h)$ and $k/1000$, respectively.

9.3. Sensitivity of the approximation error

In our first robustness test, we compute the $\|\cdot\|_\Omega$ and $\|\phi_b^{1/2} b \cdot \nabla(\cdot)\|_\Omega$ error as a function of the translation parameter δ . The manufactured solution, convection field and reaction term are

Level N	$\ e_k\ _\Omega$	EOC	$\frac{1}{2} \ b \cdot n ^{1/2} [e_k] \ _{\mathcal{F}_h}$	EOC	$\ \phi^{1/2} b \cdot \nabla e_k\ _\Omega$	EOC
0	$4.34 \cdot 10^{-1}$	—	$6.50 \cdot 10^{-2}$	—	$2.20 \cdot 10^{-1}$	—
1	$2.98 \cdot 10^{-1}$	0.54	$6.70 \cdot 10^{-2}$	-0.04	$2.29 \cdot 10^{-1}$	-0.06
2	$2.13 \cdot 10^{-1}$	0.49	$6.66 \cdot 10^{-2}$	0.01	$2.56 \cdot 10^{-1}$	-0.17
3	$1.51 \cdot 10^{-1}$	0.50	$5.21 \cdot 10^{-2}$	0.35	$2.84 \cdot 10^{-1}$	-0.15
4	$1.15 \cdot 10^{-1}$	0.39	$4.02 \cdot 10^{-2}$	0.37	$2.88 \cdot 10^{-1}$	-0.02

Table 9.2: Convergence rates for the third example with a sharp internal layer for $\epsilon = 10^{-8}$ using $\mathbb{P}_1(\mathcal{T}_k)$.

again given by (9.2). To demonstrate that the ghost penalties are necessary to render the errors insensitive to the particular cut configuration, we repeat the computation with either g_c or g_b or both turned off, setting the corresponding stabilization parameters to 0. The resulting plots

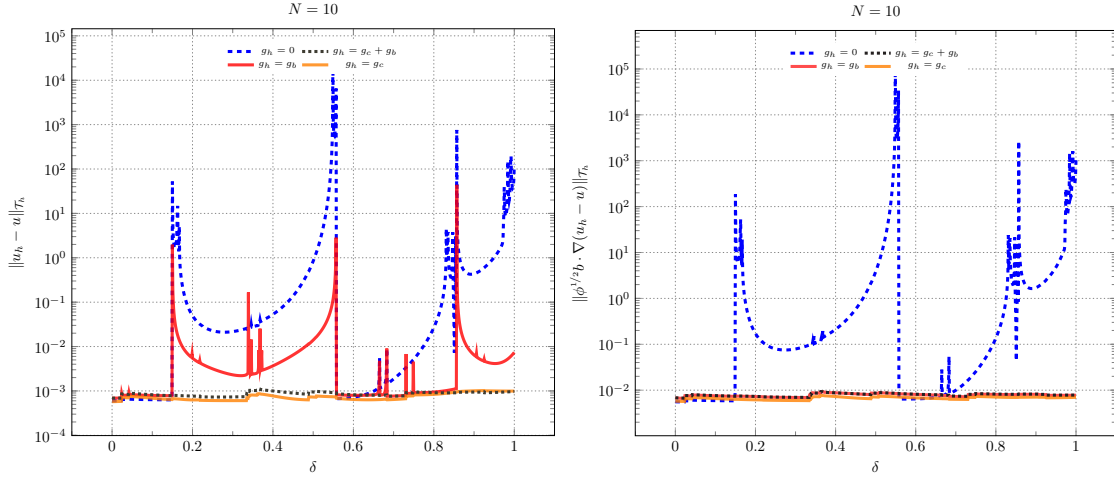


Figure 9.4: Error sensitivity for different choices of g_h in the translated circular domain test considering the L^2 (left) and streamline diffusion (right) error norm.

displayed in Figure 9.4 show that both the $\|\cdot\|_\Omega$ and $\|\phi_b^{1/2} b \cdot \nabla(\cdot)\|_\Omega$ error curves are highly erratic and exhibit large spikes when the ghost penalties are completely turned off. For the fully stabilized method on the other hand, the errors are largely insensitive to the translation parameter δ . We also observe that the L^2 error already appears to be geometrically robust when only g_c is activated, while the sole activation of g_b does not have such effect. For the streamline diffusion error, both g_b and g_c have a stabilizing effect for the particular example. The stabilizing effect of g_c can be easily explained looking at the unified ghost penalty g_h defined in (8.19) and realizing that for the given coefficients and considered coarse mesh size, we have that $c_0 \sim \frac{b_c}{h}$.

9.4. Sensitivity of the conditioning number

Using the identical setup as in Section 9.3, we now compute the condition number of the system matrix (7.1) as a function of the translation parameter δ . For the fully stabilized formulation with stabilization parameters $\beta = \gamma_0 = \gamma_1 = 0.01$, we see that the condition number changes very mildly with the position parameter δ , while for the unstabilized formulation, large spikes can be observed up to the point where the system matrix is practically singular. In a second run, we study the effect of the magnitude of the ghost penalty parameters on the magnitude and geometrical robustness of the condition number. For simplicity, we rescale all ghost penalty parameters simultaneously. Figure 9.5 (right) shows that both the base line magnitude and the fluctuation of the condition number decrease with increasing size of the stability parameters with

a minimum for some $\beta_0 = \gamma_0 = \gamma_1 \in [0.01, 1]$. A further increase of the stability parameters leaves the condition number insensitive to δ , but leads to an increase of the overall magnitude. Combined with a series of convergence experiments (not presented here) for various parameter choices and combinations, we found that our parameter choice $\beta = \gamma_0 = \gamma_1 = 0.01$ offers a good balance between the accuracy of the numerical scheme and the magnitude and fluctuation of the condition number.

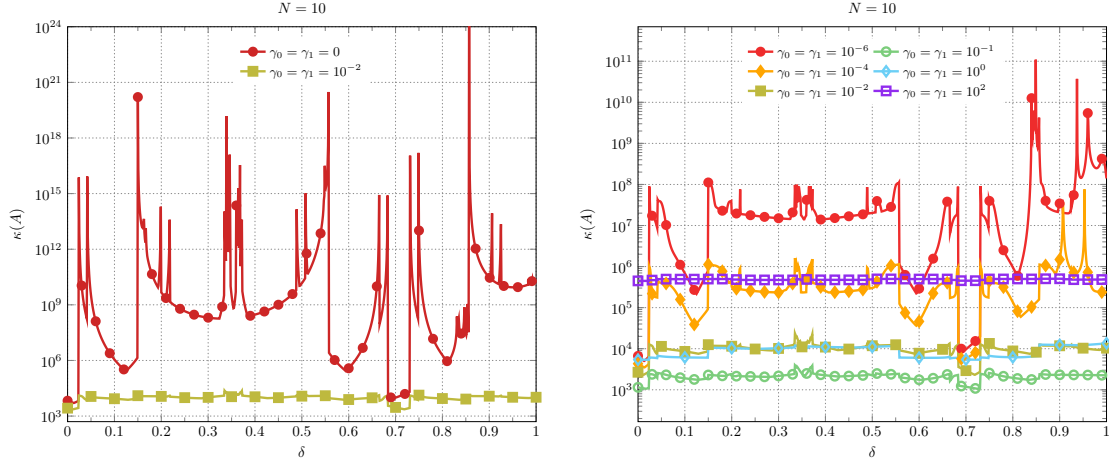


Figure 9.5: (Left) Condition number sensitivity for the translated domain test with and without ghost penalty stabilization g_c . (Right) Condition number sensitivity for changing values of the stabilization parameters γ_0 and γ_1 .

Acknowledgments

The authors gratefully acknowledge financial support from the Kempe Foundation, Postdoc Scholarship JCK-1612, and from the Swedish Research Council under Starting Grant 2017-05038.

References

- [1] C. Gürkan, A. Massing, A stabilized cut discontinuous Galerkin framework: I. Elliptic boundary value and interface problems, ArXiv e-prints .
- [2] F. Dassi, S. Perotto, L. Formaggia, P. Ruffo, Efficient geometric reconstruction of complex geological structures, Math. Comput. Simul 106 (2014) 163–184.
- [3] L. Antiga, J. Peiró, D. A. Steinman, From image data to computational domains, in: Cardiovascular Mathematics, Springer, 123–175, 2009.
- [4] L. Cattaneo, P. Zunino, Computational models for fluid exchange between microcirculation and tissue interstitium, Networks and Heterogeneous Media 9 (1).
- [5] T. E. Tezduyar, S. Sathe, R. Keedy, K. Stein, Space–time finite element techniques for computation of fluid–structure interactions, Comput. Methods Appl. Mech. Engrg. 195 (17) (2006) 2002–2027.
- [6] W. A. Wall, A. Gerstenberger, P. Gamnitzer, C. Förster, E. Ramm, Large deformation fluid–structure interaction—advances in ALE methods and new fixed grid approaches, in: Fluid–structure interaction, Springer, 195–232, 2006.

- [7] J. Baiges, R. Codina, The fixed-mesh ALE approach applied to solid mechanics and fluid-structure interaction problems, *Int. J. Numer. Methods Eng.* 81 (2009) 1529–1557.
- [8] A. MR, O. K., Moving boundary-moving mesh analysis of phase change problems using finite elements and transfinite mappings, *Int. J. Numer. Methods Eng.* 23 (1986) 591–607.
- [9] S. Groß, V. Reichelt, A. Reusken, A finite element based level set method for two-phase incompressible flows, *Computing and Visualization in Science* 9 (4) (2006) 239–257.
- [10] E. Marchandise, J.-F. Remacle, A stabilized finite element method using a discontinuous level set approach for solving two phase incompressible flows, *J. Comp. Phys.* 219 (2) (2006) 780–800.
- [11] S. Ganesan, L. Tobiska, A coupled arbitrary Lagrangian–Eulerian and Lagrangian method for computation of free surface flows with insoluble surfactants, *J. Comput. Phys.* 228 (8) (2009) 2859–2873.
- [12] G. Allaire, C. Dapogny, P. Frey, Shape optimization with a level set based mesh evolution method, *Comput. Methods Appl. Mech. Engrg.* 282 (2014) 22–53.
- [13] E. Burman, D. Elfverson, P. Hansbo, M. G. Larson, K. Larsson, Shape optimization using the cut finite element method, *Comput. Methods Appl. Mech. Engrg.* 328 (2018) 242–261.
- [14] A. Bernland, E. Wadbro, M. Berggren, Acoustic shape optimization using cut finite elements, *Int. J. Numer. Methods Eng.* 113 (2017) 432–449.
- [15] S. Bordas, E. Burman, M. Larson, M. Olshanskii (Eds.), *Geometrically Unfitted Finite Element Methods and Applications*, Springer, 2018.
- [16] A. Gerstenberger, W. A. Wall, An extended finite element method/Lagrange multiplier based approach for fluid–structure interaction, *Comput. Methods Appl. Mech. Engrg.* 197 (19) (2008) 1699–1714.
- [17] S. Court, M. Fournié, A. Lozinski, A fictitious domain approach for Fluid-Structure Interactions based on the eXtended Finite Element Method, *ESAIM: Proceedings and Surveys* 45 (2014) 308–317.
- [18] E. Burman, P. Hansbo, Fictitious domain finite element methods using cut elements: I. A stabilized Lagrange multiplier method, *Comput. Methods Appl. Mech. Engrg.* 199 (2010) 2680–2686.
- [19] E. Burman, P. Hansbo, Fictitious domain finite element methods using cut elements: II. A stabilized Nitsche method, *Appl. Numer. Math.* 62 (4) (2012) 328–341.
- [20] E. Burman, P. Zunino, Numerical approximation of large contrast problems with the unfitted Nitsche method, *Front. Numer. Anal.* 2010 (2012) 1–54.
- [21] J. Guzman, M. A. Sanchez, M. Sarkis, A finite element method for high-contrast interface problems with error estimates independent of contrast, *ArXiv e-prints* .
- [22] E. Burman, J. Guzmán, M. A. Snchez, M. Sarkis, Robust flux error estimation of an unfitted Nitsche method for high-contrast interface problems, *IMA J. Numer. Anal.* .
- [23] E. Burman, P. Hansbo, Fictitious domain methods using cut elements: III. A stabilized Nitsche method for Stokes’ problem, *ESAIM: Math. Model. Numer. Anal.* 48 (3) (2014) 859–874.
- [24] A. Massing, M. G. Larson, A. Logg, M. E. Rognes, A stabilized Nitsche overlapping mesh method for the Stokes problem, *Numer. Math.* 128 (1) (2014) 73–101.

- [25] E. Burman, S. Claus, A. Massing, A Stabilized Cut Finite Element Method for the Three Field Stokes Problem, *SIAM J. Sci. Comput.* 37 (4) (2015) A1705–A1726.
- [26] L. Cattaneo, L. Formaggia, G. F. Iori, A. Scotti, P. Zunino, Stabilized extended finite elements for the approximation of saddle point problems with unfitted interfaces, *Calcolo* (2014) 1–30.
- [27] A. Massing, B. Schott, W. Wall, A stabilized Nitsche cut finite element method for the Oseen problem, *Comput. Methods Appl. Mech. Engrg.* 328 (2018) 262–300.
- [28] M. Winter, B. Schott, A. Massing, W. Wall, A Nitsche cut finite element method for the Oseen problem with general Navier boundary conditions, *Comput. Methods Appl. Mech. Engrg.* 330 (2017) 220–252.
- [29] M. Kirchhart, S. Groß, A. Reusken, Analysis of an XFEM discretization for Stokes interface problems, *SIAM J. Sci. Comput.* 38 (2) (2016) A1019–A1043.
- [30] S. Groß, T. Ludescher, M. Olshanskii, A. Reusken, Robust preconditioning for XFEM applied to time-dependent Stokes problems, *SIAM J. Sci. Comput.* 38 (6) (2016) A3492–A3514.
- [31] J. Guzmán, M. Olshanskii, Inf-sup stability of geometrically unfitted Stokes finite elements, To appear in *Math. Comp.* .
- [32] B. Schott, U. Rasthofer, V. Gravemeier, W. A. Wall, A face-oriented stabilized Nitsche-type extended variational multiscale method for incompressible two-phase flow, *Int. J. Numer. Methods Eng.* 104 (7) (2015) 721–748.
- [33] S. Groß, A. Reusken, Numerical methods for two-phase incompressible flows, vol. 40, Springer, 2011.
- [34] A. Massing, M. G. Larson, A. Logg, M. Rognes, A Nitsche-based cut finite element method for a fluid-structure interaction problem, *Commun. Appl. Math. Comput. Sci.* 10 (2) (2015) 97–120.
- [35] B. Flemisch, A. Fumagalli, A. Scotti, A Review of the XFEM-Based Approximation of Flow in Fractured Porous Media, in: *Advances in Discretization Methods: Discontinuities, Virtual Elements, Fictitious Domain Methods*, vol. 12, Springer, 47–76, 2016.
- [36] A. Fumagalli, Numerical modelling of flows in fractured porous media by the XFEM method, Ph.D. thesis, Italy, 2012.
- [37] C. D’Angelo, A. Scotti, A mixed finite element method for Darcy flow in fractured porous media with non-matching grids, *ESAIM: Math. Model. Numer. Anal.* 46 (02) (2012) 465–489.
- [38] L. Formaggia, A. Fumagalli, A. Scotti, P. Ruffo, A reduced model for Darcy’s problem in networks of fractures, *ESAIM: Math. Model. Numer. Anal.* 48 (4) (2013) 1089–1116.
- [39] J. Parvizia, A. Düster, E. Rank, Finite cell method, *Comput. Mech.* 41 (1) (2007) 121–133.
- [40] F. Xu, D. Schillinger, D. Kamensky, V. Varduhn, C. Wang, M.-C. Hsu, The tetrahedral finite cell method for fluids: Immersogeometric analysis of turbulent flow around complex geometries, *Comput. Fluids* 141 (2016) 135–154.
- [41] V. Varduhn, M.-C. Hsu, M. Ruess, D. Schillinger, The tetrahedral finite cell method: Higher-order immersogeometric analysis on adaptive non-boundary-fitted meshes, *Int. J. Numer. Meth. Engng.* 107 (2016) 1054–1079.
- [42] D. Schillinger, M. Ruess, The finite cell method: A review in the context of higher-order structural analysis of cad and image-based geometric models, *Arch. Comput. Methods Eng.* (2014) 1–65.

- [43] P. Bastian, C. Engwer, An unfitted finite element method using discontinuous Galerkin, *Internat. J. Numer. Meth. Engrg* 79 (12) (2009) 1557–1576.
- [44] P. Bastian, C. Engwer, J. Fahlke, O. Ippisch, An Unfitted Discontinuous Galerkin method for pore-scale simulations of solute transport, *Math. Comput. Simul* 81 (10) (2011) 2051–2061.
- [45] R. I. Saye, High-Order Quadrature Methods for Implicitly Defined Surfaces and Volumes in Hyperrectangles, *SIAM J. Sci. Comput.* 37 (2) (2015) A993–A1019.
- [46] W. E. H. Solle, O. Bokhove, J. J. W. van der Vegt, Space–time discontinuous Galerkin finite element method for two-fluid flows, *J. Comput. Phys.* 230 (3) (2011) 789–817.
- [47] F. Heimann, C. Engwer, O. Ippisch, P. Bastian, An unfitted interior penalty discontinuous Galerkin method for incompressible Navier–Stokes two-phase flow, *Internat. J. Numer. Methods Fluids* 71 (3) (2013) 269–293.
- [48] R. Saye, Implicit mesh discontinuous Galerkin methods and interfacial gauge methods for high-order accurate interface dynamics, with applications to surface tension dynamics, rigid body fluid-structure interaction, and free surface flow: Part I, *J. Comput. Phys.* 344 (2017) 647–682.
- [49] B. Müller, S. Krämer-Eis, F. Kummer, M. Oberlack, A high-order Discontinuous Galerkin method for compressible flows with immersed boundaries, *Int. J. Numer. Methods Eng.* 110 (1) (2016) 3–30, nme.5343.
- [50] D. Krause, F. Kummer, An Incompressible Immersed Boundary Solver for Moving Body Flows using a Cut Cell Discontinuous Galerkin Method, *Comput. Fluids* 153 (2017) 118–129.
- [51] F. Kummer, Extended discontinuous Galerkin methods for two-phase flows: the spatial discretization, *Internat. J. Numer. Meth. Engrg* 109 (2) (2017) 259–289.
- [52] S. Badia, F. Verdugo, A. F. Martín, The aggregated unfitted finite element method for elliptic problems, *arXiv preprint arXiv:1709.09122* .
- [53] S. Badia, F. Verdugo, Robust and scalable domain decomposition solvers for unfitted finite element methods, *J. Comput. Appl. Math.* .
- [54] R. Massjung, An unfitted discontinuous Galerkin method applied to elliptic interface problems, *SIAM J. Numer. Anal.* 50 (6) (2012) 3134–3162.
- [55] A. Johansson, M. Larson, A High Order Discontinuous Galerkin Nitsche Method for Elliptic Problems with Fictitious Boundary, *Numer. Math.* 123 (4).
- [56] E. Burman, P. Hansbo, M. G. Larson, S. Zahedi, Stabilized CutFEM for the convection problem on surfaces, *arXiv preprint arXiv:1511.02340* (2015) 1–32.
- [57] M. A. Olshanskii, A. Reusken, X. Xu, A stabilized finite element method for advection–diffusion equations on surfaces, *IMA J. Numer. Anal.* 34 (2) (2014) 732–758.
- [58] E. Burman, P. Hansbo, M. G. Larson, A. Massing, S. Zahedi, A Stabilized Cut Streamline Diffusion Finite Element Method for Convection-Diffusion Problems on Surfaces, *ArXiv e-prints* .
- [59] W. Reed, T. Hill, Triangular Mesh Methods for the Neutron Transport Equation, Technical Report LA-UR-73-479, Los Alamos Scientific Laboratory, Los Alamos, NM .
- [60] P. Lesaint, P. Raviart, On a finite element method for solving the neutron transport equation. In: *Mathematical Aspects of Finite Elements in Partial Differential Equations (Proc. Sympos., Math. Res.Center, Univ. Wisconsin, Madison, Wis., 1974)*, . Academic Press, New York 33 (1974) 89–123.

- [61] C. Johnson, U. Nävert, J. Pitkäranta, Finite element methods for linear hyperbolic problems, *Comput. Methods Appl. Mech. Engrg.* 45 (1-3) (1984) 285–312.
- [62] F. Brezzi, L. D. Marini, E. Süli, Discontinuous Galerkin methods for first-order hyperbolic problems, *Math. Models Methods Appl. Sci.* 14 (12) (2004) 1893–1903.
- [63] B. Cockburn, Discontinuous Galerkin methods for convection-dominated problems, *High-Order Methods for Computational Physics, Lect. Notes Comput. Sci. Eng.* 9 (1999) 69–224.
- [64] P. Houston, C. Schwab, E. Süli, Discontinuous hp-finite element methods for advection-diffusion-reaction problems, *SIAM J. Numer. Anal.* 39 (6) (2002) 2133–2163.
- [65] H. Zarin, H.-G. Roos, Interior penalty discontinuous approximations of convection–diffusion problems with parabolic layers, *Numer. Math.* 100 (2005) 735–759.
- [66] D. Arnold, F. Brezzi, B. Cockburn, L. Marini, Unified analysis of discontinuous Galerkin methods for elliptic problems, *SIAM J. Num. Anal.* 39 (2002) 1749–1779.
- [67] B. F., M. G., M. D., P. P., R. A., Discontinuous Galerkin approximations for elliptic problems, *Numerical Methods for Partial Differential Equations* 16 (4) (2000) 365–378.
- [68] D. A. Di Pietro, A. Ern, *Mathematical aspects of discontinuous Galerkin methods*, vol. 69, Springer, 2012.
- [69] J. S. Hesthaven, T. Warburton, *Nodal discontinuous Galerkin methods: algorithms, analysis, and applications*, Springer Science & Business Media, 2007.
- [70] C. Gürkan, F. Heimann, C. Lehrenfeld, A. Massing, A stabilized cut discontinuous Galerkin framework: III. Surface and mixed dimensional coupled problems, In preparation. .
- [71] E. Burman, P. Hansbo, M. G. Larson, A. Massing, A cut discontinuous Galerkin method for the Laplace–Beltrami operator, *IMA J. Numer. Anal.* 37 (1) (2016) 138–169.
- [72] A. Massing, A Cut Discontinuous Galerkin Method for Coupled Bulk-Surface Problems, chap. Chapter in UCL Workshop volumen on ”Geometrically Unfitted Finite Element Methods”, to appear in *Lecture Notes in Computational Science and Engineering*, Springer, 1–19, 2017.
- [73] E. Burman, S. Claus, P. Hansbo, M. G. Larson, A. Massing, CutFEM: discretizing geometry and partial differential equations, *Internat. J. Numer. Meth. Engrg* 104 (7) (2015) 472–501.
- [74] B. Müller, F. Kummer, M. Oberlack, Highly accurate surface and volume integration on implicit domains by means of moment-fitting, *Internat. J. Numer. Meth. Engrg* 6 (2013) 10–16.
- [75] C. Lehrenfeld, High order unfitted finite element methods on level set domains using isoparametric mappings, *Comput. Methods Appl. Mech. Engrg.* 300 (2016) 716–733.
- [76] T.-P. Fries, S. Omerović, Higher-order accurate integration of implicit geometries, *Int. J. Numer. Methods Eng.* 106 (2016) 323–371.
- [77] T. Fries, S. Omerović, D. Schöllhammer, J. Steidl, Higher-order meshing of implicit geometries Part I: Integration and interpolation in cut elements, *Comput. Methods Appl. Mech. Engrg.* 313 (2017) 759–784.
- [78] A. Hansbo, P. Hansbo, M. G. Larson, A Finite Element Method on Composite Grids based on Nitsche’s Method, *ESAIM: Math. Model. Numer. Anal.* 37 (3) (2003) 495–514.
- [79] E. Stein, *Singular Integrals and Differentiability Properties of Functions*, Princeton University Press, 1970.

- [80] A. Ern, J.-L. Guermond, Discontinuous Galerkin methods for Friedrichs' systems. I. General theory, *SIAM J. Numer. Anal.* 44 (2) (2006) 753–778.
- [81] D. A. Di Pietro, A. Ern, J.-L. Guermond, Discontinuous Galerkin methods for anisotropic semidefinite diffusion with advection, *SIAM J. Numer. Anal.* 46 (2) (2008) 805–831.
- [82] J. Li, J. Melenk, B. Wohlmuth, J. Zou, Optimal a priori estimates for higher order finite elements for elliptic interface problems, *Appl. Numer. Math.* 60 (1) (2010) 19–37.
- [83] E. Burman, P. Hansbo, M. Larson, S. Zahedi, Cut Finite Element Methods for Coupled Bulk-Surface Problems, *Numer. Math.* 133 (2016) 203–231.
- [84] S. Groß, M. A. Olshanskii, A. Reusken, A trace finite element method for a class of coupled bulk-interface transport problems, *ESAIM: Math. Model. Numer. Anal.* 49 (5) (2015) 1303–1330.
- [85] A. Ern, J.-L. Guermond, Evaluation of the condition number in linear systems arising in finite element approximations, *ESAIM: Math. Model. Numer. Anal.* 40 (1) (2006) 29–48.
- [86] R. Becker, E. Burman, P. Hansbo, A Nitsche extended finite element method for incompressible elasticity with discontinuous modulus of elasticity, *Comput. Methods Appl. Mech. Engrg.* 198 (41-44) (2009) 3352–3360.
- [87] E. Burman, Ghost penalty, *C.R. Math.* 348 (21-22) (2010) 1217–1220.
- [88] A. Massing, M. Larson, A. Logg, M. Rognes, A stabilized Nitsche fictitious domain method for the Stokes problem, *J. Sci. Comput.* 61 (3) (2014) 604–628.
- [89] J. Preuß, J.-P. D. C. Lehrenfeld, G. Lube, Higher order unfitted isoparametric space-time FEM on moving domains, Master's thesis, masters thesis, NAM, University of Göttingen, 2018.
- [90] P. Houston, C. Schwab, E. Süli, Stabilized hp-finite element methods for first-order hyperbolic problems, *SIAM Journal on Numerical Analysis* 37 (5) (2000) 1618–1643.
- [91] T. E. Peterson, A note on the convergence of the discontinuous Galerkin method for a scalar hyperbolic equation, *SIAM J. Numer. Anal.* 28 (1) (1991) 133–140.
- [92] E. Burman, A unified analysis for conforming and nonconforming stabilized finite element methods using interior penalty, *SIAM J. Numer. Anal.* 43 (5) (2005) 2012–2033.